NATIONAL AERONAUTICS AND SPACE ADMINISTRATION

Technical Report 32-1561

Stability Evaluation of a Rocket Engine for Gaseous Oxygen Difluoride (OF_2) and Gaseous Diborane (B_2H_6) Propellants

Richard M. Clayton

JET PROPULSION LABORATORY
CALIFORNIA INSTITUTE OF TECHNOLOGY
PASADENA, CALIFORNIA

August 15, 1972

NATIONAL AERONAUTICS AND SPACE ADMINISTRATION

Technical Report 32-1561

Stability Evaluation of a Rocket Engine for Gaseous Oxygen Difluoride (OF_2) and Gaseous Diborane (B_2H_6) Propellants

Richard M. Clayton

JET PROPULSION LABORATORY
CALIFORNIA INSTITUTE OF TECHNOLOGY
PASADENA, CALIFORNIA

August 15, 1972

Preface

The work described in this report was performed by the Propulsion Division of the Jet Propulsion Laboratory.

Acknowledgment

The author wishes to acknowledge the contributions of Dr. R. O. Kushida in carrying out the computer simulations of unstable combustion, of Mr. F. G. Gerbracht in design and fabrication support, and of Mr. J. W. Short and Mr. T. L. Nielsen in test operation support.

Contents

Tables

Contents (contd)

Figures

Abstract

Results of an experimental evaluation of the dynamic stability of a candidate combustor for the space storable propellants gaseous OF_2/B_2H_6 show that the combustor is unstable without supplementary damping. An analysis using a Jet Propulsion Laboratory computer program (TRDL) indicated that the uninhibited engine could be unstable. The experiments, conducted with O_2/C_2H_4 substitute propellants and with 70-30 FLOX/B_2H_6 (OF_2 simulated with FLOX), show that the uninhibited combustor has a low stability margin to starting transient perturbations, but that it is relatively insensitive to bomb disturbances. Damping cavities are shown to provide stability.

Stability Evaluation of a Rocket Engine for Gaseous Oxygen Difluoride (OF_2) and Gaseous Diborane (B_2H_6) Propellants

I. Introduction

Unmanned deep-space missions have fostered interest in the development of propulsion systems to utilize the so-called space storable propellant combinations. And because engine development experiences over the past decade have shown that combustion instability is likely to be a continuing problem, plaguing nearly all new combustor development, it is deemed essential that candidate design concepts be evaluated for stability in a timely manner.

To that end, the stability characteristics of a 4.45-kN (1000-lbf) thrust engine for use with oxygen difluoride (OF_2) and diborane (B_2H_6) propellants have been evaluated. This combustor represents a design concept for potential use in future spacecraft systems and is being evaluated elsewhere for its capability for long-duration burn times (Ref. 1). The primary emphasis in the experiments conducted at the Jet Propulsion Laboratory (JPL) was on dynamic stability with bombed firings of the combustor.

A unique feature of the engine from a combustion standpoint is that both propellants are vaporized in thrust chamber coolant passages and therefore enter the injector and are injected as gases. Thus, mixing and combustion take place entirely through gas phase processes, except for the possibility of two-phase flow during starting transients.

Experience has shown that solid combustion products can accumulate with time on the interior surfaces of the combustor with OF_2/B_2H_6 propellants, though this problem appears to be much less severe with gaseous reactants, compared with liquid reactants. Thus even though the engine was designed with damping cavities, it was considered necessary to evaluate the stability characteristics of the uninhibited engine as well, since deposits accumulated over burn times approaching 1000 s (foreseen for future JPL flight missions) could render the cavities ineffective.

A relatively small-scale analytical effort utilized a computer program (TRDL) which solves numerically the

unsteady, two-dimensional nonlinear equations of motion for a gas with internal mass and energy sources (Ref. 2). Arbitrary initial disturbances were imposed on the steady state solutions to simulate dynamic stability experiments.

The experimental work was undertaken in two parts:

(1) Preliminary experiments in which the substitute propellants, gaseous oxygen and ethylene (C_2H_4), were utilized in order to minimize complexities associated with studies with deeply cryogenic propellants.

(2) Confirmation experiments in which FLOX (70% F_2/30% O_2 by weight) and B_2H_6 were utilized to verify the preliminary results. This FLOX mixture is commonly used to simulate OF_2 in rocket experiments.

II. Engine Description

The regeneratively cooled thrust chamber utilizes a double panel concept, with the B_2H_6 being the primary and the OF_2 the secondary coolant. An artist's rendition of the engine concept is shown in Fig. 1, omitting the details of design and fabrication, which may be found in Ref. 1. Both propellants enter coolant passages in the nozzle skirt as liquids. The B_2H_6 is introduced at an area ratio of 20 and flows toward the injector through the innermost of the double panel passages. The OF_2 is introduced at an area ratio of 10 and flows toward the injector through the outermost passages. Both propellants are fully vaporized before reaching the injector. Nominal design conditions for the engine are listed in Table 1.

The injector comprises a barrier fuel flow injected from 80 shower head orifices located adjacent to the chamber

Table 1. Nominal design conditions for regeneratively cooled OF_2/B_2H_6 engine

Parameter	Value
Chamber pressure	689.5 kN/m^2 (100 psia)
Nozzle expansion ratio	60:1
Vacuum thrust	4.448 kN (1000 lbf)
Vacuum specific impulse	3.970 kN-s/kg (405 lbf-s/lbm)
Mixture ratio (O/F)	3:1
Total flow rate	1.120 kg/s (2.469 lbm/s)
Barrier fuel flow	8% of total flow
Average chamber mass flux	83.66 kg/s-m^2 (0.119 lbm/s-in.^{2})
Chamber inside diameter	13.21 cm (5.20 in.)
Chamber length (injector face to nozzle throat)	24.13 cm (9.50 in.)
Chamber contraction ratio	4.0:1

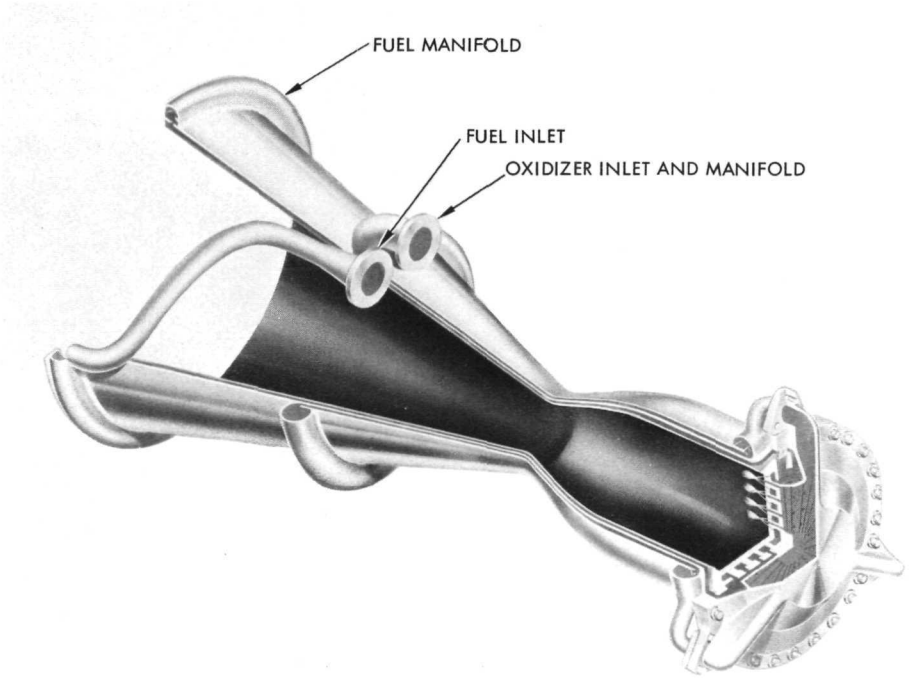

Fig. 1. Artist's conception of regeneratively cooled engine for OF_2/B_2H_6

Table 2. Nominal design conditions for OF_2/B_2H_6 injector

Parameter	Oxidizer			Core fuel			Barrier fuel		
Mass flow rate[a], kg/s (lbm/s)	0.858	(1.89)		0.195	(0.43)		0.098	(0.20)	
Pressure drop[a], kN/m^2 (psid)	234	(34)		152	(22)		152	(22)	
Orifice diameter, mm (in.) [No. of orifices]									
Rows 1–3	2.49	(0.098)	[56]	0.99	(0.039)	[112]		–	
Row 4	2.16	(0.086)	[40]	1.18	(0.047)	[80]		–	
Barrier row		–			–		1.18	(0.047)	[80]
Injection velocity, m/s (ft/s) [Mach number]	244	(800)	[0.8]	183	(600)	[0.6]	183	(600)	[0.6]
Inlet temperature[a], K (°F)	261	(10)		394	(250)		394	(250)	
Orifice L/D	11			10			7		
Orifice entry contour		Sharp			Sharp			Sharp	
Included impingement angle, rad (deg)			0.525	(30)				–	
Impingement distance from face, cm (in.)			1.525	(0.60)				–	

[a]Based on FLOX simulation of OF_2. All other values are for OF_2 design conditions.

walls and a bipropellant core flow injected from 96 triplet impinging elements (two fuel on one oxidizer) arranged in four concentric rows about the chamber axis. The triplet elements in the inner three rows are of identical configuration, but the elements in row 4 have smaller oxidizer orifices and larger fuel orifices to provide a reduced mixture ratio near the outer periphery of the core flow. The calculated radial mass and mixture ratio distributions for design flows are depicted in Fig. 2, which also shows a photograph of the injector as used in the JPL evaluation.[1] Nominal injector design conditions are listed in Table 2.

[1]The injector used in the JPL evaluation incorporated the revised oxidizer orifice diameters used in the final version (unit No. 2) of the study under Contract NAS7-765 (Ref. 1).

Provisions for damping cavities of a quarter-wave slot configuration were included in the engine design. These devices were to be located along a 0.785-rad (45-deg) conical interface at the juncture of the chamber and injector,[2] where ten equally spaced cavities, each 2.18 cm deep × 3.81 cm wide × 0.33 cm high (0.86 × 1.50 × 0.13 in.), comprise a total open area of ~ 10% of the chamber cross sectional area. The devices were designed (Ref. 1) for tuned operation at 6200 Hz, the fundamental tangential mode frequency of the combustion chamber, and the dimensions were based on an assumed cavity gas temperature of 990 K (1320°F).

[2]See Figs. 4 and 10.

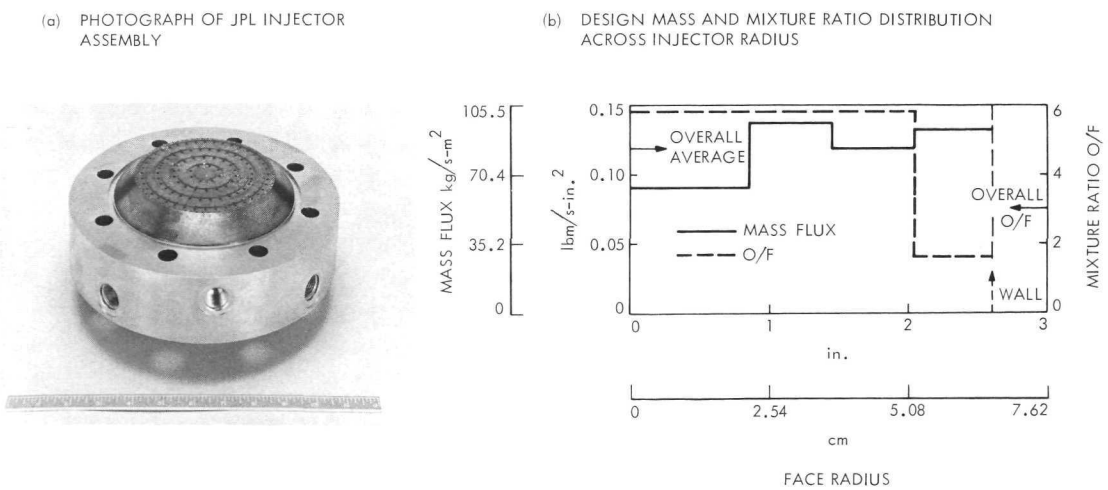

Fig. 2. Injector for OF_2/B_2H_6 engine

III. Analytic Simulation

To obtain further experience in analytic simulation of unstable rocket combustion and to provide analytic results for comparison with experimental results for the OF_2/B_2H_6 combustor, the computer program TRDL (Ref. 2) was used. The program utilizes a two-step, finite-difference numerical method to solve the equations of gas motion for the mass density, the transverse momentum flux, the axial momentum flux, and the total energy density. The combustor geometry is that of a circularly cylindrical annulus with propellant injection at one end and a convergent–divergent slot nozzle at the other end. Although baffles can be simulated in the program, cavities cannot—at present. Therefore, results were obtained only for an uninhibited model of the OF_2/B_2H_6 engine. The important dimensions used in applying the analysis to this engine are the chamber contraction ratio (4.0), chamber length (taken to be 30.5 cm or 12.0 in.), chamber diameter (13.2 cm or 5.2 in.), and the nozzle contour.

No attempt was made to model the gaseous combustion processes that, for the subject OF_2/B_2H_6 engine, are presumed to be controlled by turbulent mixing. However, a reasonable axial energy release profile was established in order to provide a steady state initial condition upon which arbitrary disturbances were imposed. At the start

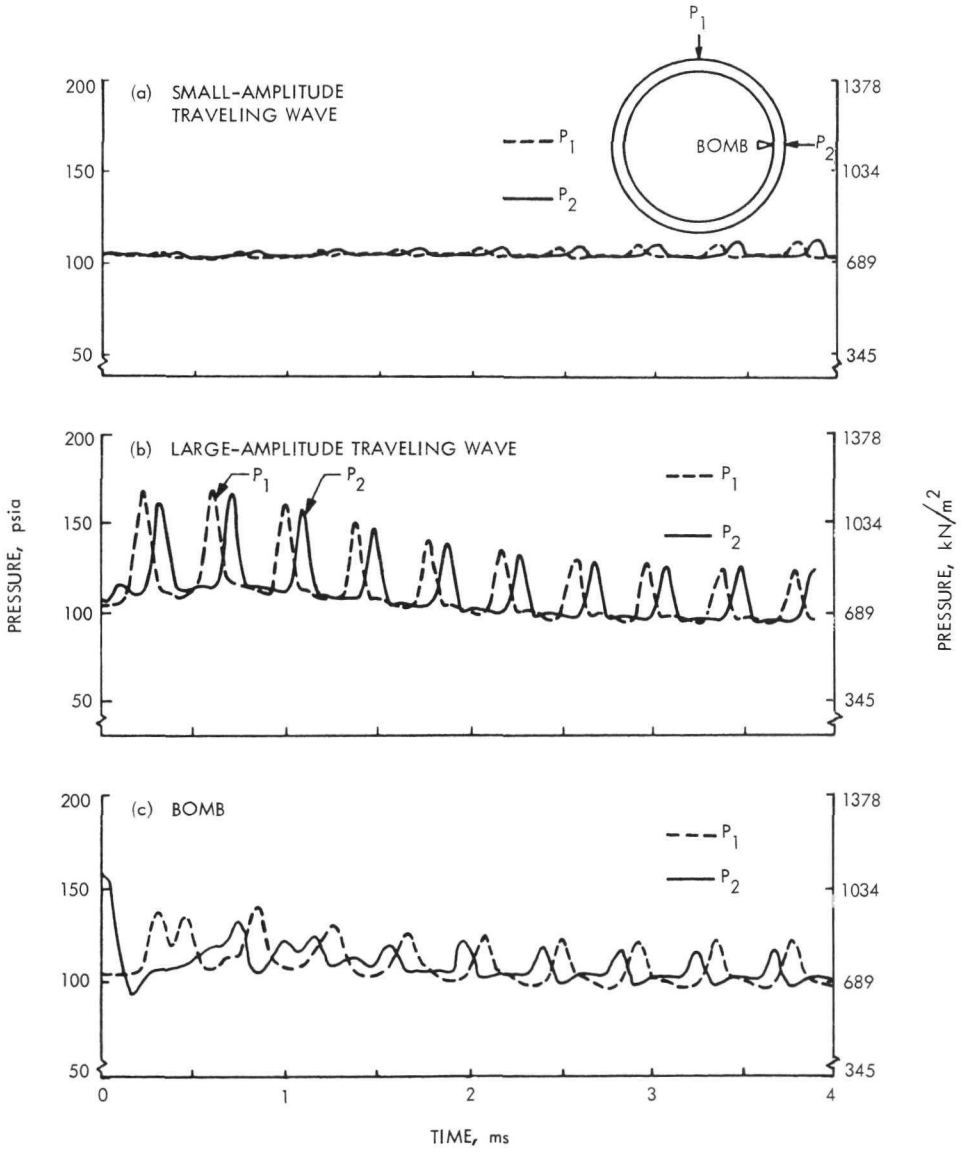

Fig. 3. Analytically observed resonance, computer simulation of OF_2/B_2H_6 engine

of the nonsteady calculations, a mass and energy release rate directly proportional to the local static pressure was arbitrarily assigned.

Chamber gas oscillations were initiated either with a steady tangentially traveling wave or with a simulated bomb. Since the computer program is limited to only two space dimensions, the region included in the simulation was the outermost region close to the chamber wall. The transverse frequencies observed analytically are of course those for the annular geometry, but this is not believed to affect the coupling of mass and energy release and gas dynamics in a significant way in the present application of the analysis, where combustion response was assumed to be independent of frequency.

The results of the analytic study are summarized in Fig. 3. The static pressure at stations 1.3 cm (0.5 in.) downstream from the injector face and 1.57 rad (90 deg) apart are depicted. In Fig. 3a, an initial small amplitude, tangentially traveling wave is seen to amplify with time. The growth rate is approximately linear from its original amplitude of 20.6 kN/m^2 peak-to-peak (3 psi) imposed on a steady chamber pressure of 689 kN/m^2 (100 psi). The growth of the small wave would indicate that the simulated bare combustor is linearly unstable.

In Fig. 3b, the initial disturbance was a stronger tangentially traveling wave of 1205 kN/m^2 peak-to-peak (175 psi) amplitude. This wave, after some initial oscillations, appears to decay toward what appears to be a limiting amplitude for a steady resonant oscillation.

The decay to a steady resonance is more rapid in the case of an initial bomb-like pressure pulse disturbance, as shown in Fig. 3c. The bomb was placed near pressure tap P_2. A "shutter" was placed adjacent to the bomb to force motion in the opposite tangential direction relative to those shown before. This shutter was removed 0.5 ms after the simulated bomb explosion. The steady resonant oscillation of approximately 179 kN/m^2 (26 psi) peak-to-peak amplitude is attained at the simulated time of 4 ms. The observed frequency of 2440 Hz corresponds closely to the expected first tangential wave frequency for the annulus dimensions and gas properties used for the analysis.

These limited analytical results with an ad hoc energy release model do not necessarily constitute a prediction of the stability of the experimental engine. However, they do demonstrate that the TRDL program is numerically stable and can produce nonlinear gas dynamic solutions that approach the wave forms, frequencies (within the limits of the annular geometry), and transitional behavior which are generally observed experimentally. Certain experimental results described below support this conclusion and thus we are encouraged to continue the development of the program.

IV. Experimental Apparatus and Techniques

A. Combustor

A heavyweight, uncooled version of the engine was fabricated by JPL using the internal dimensions of the thrust chamber and detailed injector fabrication drawings generated under contract NAS 7-765 (Ref. 1).

The internal dimensions and layout of the combustor as used at JPL are shown schematically in Fig. 4. Optional chamber lengths were provided by appropriate combinations of three chamber sections. The location of optional damping cavities in a common chamber section adjacent to the injector is also shown.[3] The cavities were not used whenever the stability of the uninhibited combustor was to be evaluated (i.e., a blank chamber section was substituted).

B. Bombing Scheme

A port for inserting an electrically fired bomb (see Appendix A for details) just inside the inner wall of the combustion chamber was provided in each of the three chamber sections (Fig. 4). Thus, from one to three bombs, depending on the chamber length, could be fired at preselected times during a given test. It was intended that each available bomb position be used during each engine run, with individual bombs sequenced to fire about 100 ms apart during the midportion of the test. However, this was in fact accomplished only for some of the preliminary experiments with O_2 and C_2H_4. For the FLOX/B_2H_6 tests, the bombs placed downstream of the first chamber section failed. It was apparent that the flame temperatures were high enough that the available Teflon sleeve used for thermal protection at the wall was inadequate. Thus, for these tests, a single bomb located in the first chamber section was normally fired about midrun. However, in some instances, the bomb was fired during the starting transient.

[3]The cavities are intended for placement in the injector side of the conical surface in the design (cooled) version of the engine rather than in the chamber side as was done for the JPL experiments. However, compensatory adjustments in the location of the conical surface at the time of JPL fabrication placed the cavities in the same relative position as for the cooled version.

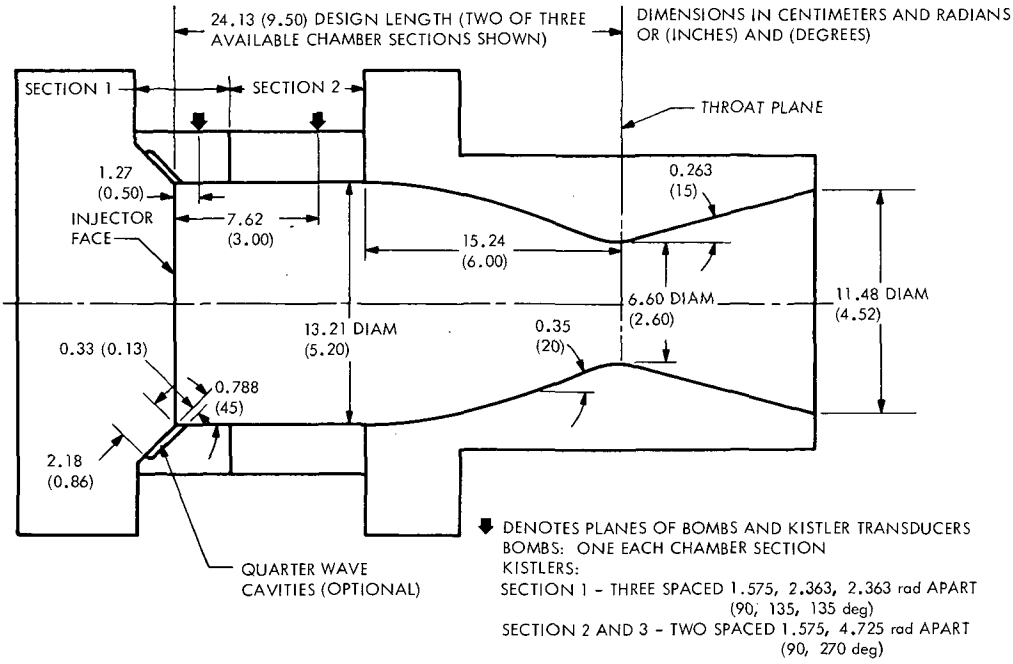

Fig. 4. Internal geometry of heavyweight OF_2/B_2H_6 engine

Bombs of 65, 130, 260, and 520 mg (1, 2, 4, and 8 grains) of PETN (pentaerythritol tetranitrate) were used during the initial experiments in order to establish pulse amplitudes and damping characteristics for various disturbance magnitudes. But eventually a charge size of 130 mg (2 grains) was adopted as standard. This charge size produced spiked initial disturbances with peak absolute amplitudes of from 2 to 3 times the mean chamber pressure.[4]

C. Instrumentation

1. High-response pressure measurements. Helium-bleed Kistler transducer taps (see Appendix B) were located as indicated in Fig. 4. All high-response data were recorded on high-speed analog tape for later playback to an oscillograph. The positional array of the transducers on the chamber boundary[5] permitted evaluation of the modes of gas motion during oscillatory combustion when the frequency and phase relationships of the simultaneously recorded transducer signals were analyzed. Typical recording, playback, and analysis techniques are discussed in Ref. 4. Response of the helium-bleed taps was estimated to be useful to 10–15 kHz from shock wave tests (see Ref. 5).

2. Flow measurements. The flow rates of the gaseous propellants supplied to the core and barrier sections of the injector were separately measured with sonic venturis located in the feed lines. The pressure and temperature of the flowing gases in each of the three systems immediately upstream of the venturis were digitally recorded throughout each firing for subsequent data reduction. The data reduction procedures which accounted for real gas effects where necessary are described in Appendix B.

3. Other measurements. In addition to the measurements discussed above, other measurements including injector manifold pressures and temperatures, damping cavity gas temperatures, and chamber pressure measurements, from which the steady state operating conditions of the combustor could be determined, were digitally recorded. These measurements were obtained by conventional methods and will not be further described here. For the interested reader, typical techniques of transducer installation, digital data recording, and instrumentation accuracies applicable to the present experimental program are described in Ref. 6. Performance data reduction is described in Appendix B.

D. Propellant Feed Systems

Photographic views and additional descriptions of the test facilities utilized for these experiments are presented in Appendix C. The salient features of the feed systems are

[4]See Fig. 8.

[5]Consistent with recommendations of Ref. 3.

presented below as an aid to understanding the experimental results discussed in Section V.

1. O_2/C_2H_4 system. Gaseous propellants were supplied from high-pressure bottle banks. The respective fuel and oxidizer bottles were manifolded to supply three separate feed systems: oxidizer, core fuel, and barrier fuel. The feed pressure to each system was separately regulated to afford flow rate control by means of adjustable pressure regulators. The sonic venturis were located in each system downstream of the regulators and just upstream of propellant shutoff valves that were close-coupled to the injector inlet ports. Thus, combustor starting flow transients could be reasonably short but well controlled by pressurizing the feed lines to a preselected level and then sequencing the propellant valves to achieve the desired initial injection sequence.

In contrast to the design propellants, the O_2/C_2H_4 combination is not hypergolic under starting conditions; therefore, it was necessary to provide an auxiliary supply of ignition energy. This was accomplished with a single unlike-impinging doublet injection element utilizing N_2O_4/(50% N_2H_4, 50% unsymmetrical dimethylhydrazine) liquid propellants, placed in the wall of the chamber section nearest to the injector (see Fig. A-2). The ignitor flame was normally started about 200 ms prior to initiating the core flows and was stopped about 200 ms after core flow ignition.

2. FLOX/B_2H_6 system. An existing cryogenic test stand facility was adapted to vaporize liquid FLOX and B_2H_6 that was normally stored at the site. The FLOX (70% F_2/ 30% O_2 by weight) was supplied from a helium-pressurized liquid tank via an auxiliary tank wherein vaporization was accomplished as the oxidizer flowed through a bed of warm aluminum rivets. The gaseous FLOX system pressure was established during prerun preparations by equilibrating gas and liquid tank pressures to the desired levels. Makeup gas was generated throughout the firings to maintain a nearly constant feed pressure.

The B_2H_6 was also supplied from the stand liquid tank and was vaporized in a second auxiliary tank in essentially the same manner as the oxidizer. But, because of the decomposition characteristics of B_2H_6, it was stored as a gas for only short periods at a temperature of about 290 K (60°F). A gas tank pressure of about 4.2 MN/m² (600 psi) was established during prerun preparations, whereupon the liquid and gas systems were isolated by suitable valves. During the firings, fuel feed line pressure was controlled by a preset pressure regulator located at the gas tank outlet. The fuel was passed through a heat exchanger during the firings to elevate its temperature, thus simulating its passage through thrust chamber cooling jacket. However, the 394 K (250°F) design value (Table 2) for the fuel injector inlet temperature was never obtained with the available heat exchanger, and the firings were made with inlet temperatures ranging from 311 to 333 K (100 to 140°F).

The impact of that experimental difficulty on the stability results was not determined. However, it is noted that the starting transient for the cooled engine will also be made over a range of below-design fuel inlet temperatures; therefore, it is believed that the temperature conditions achieved were adequate for this evaluation.

Propellant shutoff valves were located upstream of the sonic venturis in both the FLOX and the B_2H_6 feed systems. Also, the heat exchanger was located upstream of the fuel venturis, which were arranged to split the fuel flow between core and barrier flows. Thus, a considerably greater effective manifold volume was present for the FLOX/B_2H_6 compared with the preliminary O_2/C_2H_4 firings. Consequently, starting transients were longer and were probably influenced somewhat by nitrogen diluent that was always present initially from purging the feed systems downstream of the propellant shutoff valves.

E. Test Conditions

Experiments were conducted utilizing O_2/C_2H_4 propellants in order to obtain a preliminary evaluation of the stability characteristics of the gaseous combustor with and without the damping cavities installed. As indicated previously, it was intended that the preliminary results would serve to identify critical operating variables influencing stability and thus reduce the number of tests required with the more difficult-to-handle and more expensive design propellants.

For the preliminary tests, the design mass flow rates (Table 2) were assumed to approximate the mass and mixture ratio distribution produced with the design propellants. Operation at the overall design mixture ratio of 3.0 also coincided closely with the theoretical maximum combustion temperature of 3440 K for O_2/C_2H_4. This compares with the theoretical combustion temperature of 3960 K for OF_2/B_2H_6 at that mixture ratio. Thus, the chamber mode frequencies with the substitute propellants were expected to be about 7% lower than for OF_2/B_2H_6. A ~20% reduction in operating chamber pressure was also expected because of the lower c^* potential of the substitute propellants at the design mixture ratio. Tests were also

made with significant variations in flow rates about the design values.

The other combustor variable explored was chamber length. One test was conducted with the minimum length of 17.8 cm (7.0 in.) and one test was made with the 30.5 cm (12.0 in.) length. These compare with the design value of 24.1 cm (9.5 in.).

The final phase of the evaluation utilizing FLOX/B_2H_6 was made over approximately the same range of mass flow rate variation as for the preliminary experiments; however, all tests were made with the design-length combustor. Tests were again performed with and without the damping cavities. Two tests were made with modified cavities to simulate deposition of solids in the cavities.

Firings with either propellant combination were normally scheduled for 2.0 to 2.5-s duration, which was sufficient time to achieve essentially steady state operating conditions. However, resonant firings were automatically terminated early by means of an "instability shutoff" device that monitored the signal from one of the Kistler transducers. Thus, damage to the combustor from prolonged periods of sustained resonance was avoided.

F. Units

English Technical System units were used for primary measurements and calculations. Conversion to International System (SI) units was done for reporting purposes only.

V. Experimental Results

A. O_2/C_2H_4 (Substitute Propellants)

A total of 25 firings were conducted using the O_2/C_2H_4 propellants. Four firings were made without the damping cavities. The remainder (21) were made with cavities of design dimensions incorporated in the combustor. Results are summarized in Table 3.

1. Firings without cavities. All the firings without cavities were spontaneously unstable. An apparently classical linear instability was consistently exhibited during the starting transient, where a small, high-frequency oscillation grew rapidly to a nonlinear spinning wave with sustained amplitudes of 1034 kN/m² (150 psi) peak-to-peak and greater and frequency of from ~5200 to ~5700 Hz. Because of the persistent, spontaneous inception of combustor resonance exhibited in these four firings, no bombs were used.

Typically, the core ignition transient and subsequent rise of chamber pressure was monotonic and extremely smooth until the mean pressure rose to 172–207 kN/m² (25–30 psig). Detailed examination of the high response records revealed that at about this point a small continuous-wave kind of oscillation developed, but there was never any indication of a discrete impulsive perturbation. An example of the inception of resonance and the nonlinear nature of the sustained first tangential spinning wave for one firing is shown in Fig. 5. Note that the linear transition to sustained resonance and the nonlinear wave form during resonance bear qualitative similarity to the computer simulation of these conditions shown in Fig. 3.

The possibility that the hypergolic liquid ignitor flame triggered the oscillations was never conclusively ruled out; however, changing the starting sequence of the injected gaseous propellants relative to each other and to the ignitor flow had no significant effect on the inception of the oscillations. The possibility that the ignitor flow was sustaining the oscillations was eliminated by the fact that the oscillations persisted without significant change after the ignitor flow stopped.

2. Firings with cavities. The subsequent installation of the damping cavities was highly effective in stabilizing the engine. A series of firings at near-design flow rates perturbed with bombs of from 65 to 520 mg (1 to 8 grains) failed to initiate sustained oscillations, exhibiting damping times[6] of less than 10 ms.[7] However, a residual oscillation of generally less than 69 kN/m² (10 psi) peak-to-peak appeared sporadically, independent of the size or time of bomb discharges. The frequency of this oscillation was ~4545 Hz.

The characteristics of the engine with cavities were not significantly altered from those described above in a series of firings with off-design flow rates and chamber lengths. All conditions were stable to the 130-mg (2-grain) bomb size, which was adopted for producing an adequate disturbance for this engine.

In these preliminary experiments with O_2/C_2H_4, no attempt was made to modify the damping effectiveness of the cavities by altering their dimensions from the design values.

---

[6]Damping time as used herein is defined as the total time (to the nearest millisecond) for chamber pressure (Kistler measurements nearest the injector face) to return to predisturbance appearance on a high time-resolution oscillograph record.

[7]See Fig. 8a.

Table 3. Results for O_2/C_2H_4 firings[a]

Run	$\dot{m}_t$ kg/s	$\dot{m}_t$ lbm/s	O/F	Z_t	$[p_{ce}]_t$ kN/m²	$[p_{ce}]_t$ psia	c_t^* m/s	c_t^* ft/s	η_{c^*} %	p_c rms kN/m²	p_c rms psi	Bomb size, mg (grain), for chamber position: Inj.	Mid.	Noz.	Damp time, ms	Resonance: Amplitude kN/m²	Amplitude psi	Frequency, Hz	Remarks
Without cavities																			
B-1351[a]	–	–	–	0	~455	~66	–	–	–	–	–	–	–	–	–	517	75	5290 to 5618	Short duration (250–600 ms) runs. Spontaneous transition to resonance during starting transient. Performance not calculated. No bombs used.
B-1352[a]	–	–	–	–	~421	~61	–	–	–	–	–	–	–	–	–	1207	175	5464 to 5682	
B-1353[a]	1.091	2.406	3.243	0.076	482.7	70.00	–	–	–	–	–	–	–	–	–	1034	150	5200 to 5464	
B-1354[a]	1.140	2.513	3.209	0.076	536.4	77.80	–	–	–	–	–	–	–	–	–	1103	160	5291 to 5376	
With cavities																			
B-1356[a]	1.205	2.657	3.140	0.0774	548.8	79.60	1560.0	5118	88.5	11.7	1.7	–	–	–	–	–	–	–	Stable. No bomb used.
B-1357	1.237	2.728	2.741	0.0844	576.6	83.62	1595.6	5235	88.5	14.5	2.1	65 (1)	–	–	5[b]	–	–	–	Stable.
B-1358	1.167	2.572	2.928	0.0807	541.6	78.55	1590.1	5217	89.2	11.7	1.7	–	–	–	–	–	–	–	Stable. No bomb used.
B-1359[a]	1.210	2.668	2.763	0.0839	565.4	82.00	1600.2	5250	88.9	15.9	2.3	–	–	520 (8)[c]	5	–	–	–	Stable.
B-1360	1.170	2.579	3.018	0.0795	541.4	78.52	1585.3	5201	89.5	15.9	2.3	65 (1)	–	–	7	–	–	–	Stable.
B-1361	1.190	2.623	3.023	0.0821	543.6	78.84	1564.8	5134	88.3	13.1	1.9	130 (2)[c]	–	–	6	–	–	–	Stable.
B-1362	1.174	2.589	2.971	0.0826	541.5	78.54	1579.5	5182	88.9	17.2	2.5	260 (4)	–	–	9	–	–	–	Stable.
B-1363	1.103	2.432	3.195	0.0747	508.2	73.70	1577.9	5177	89.9	13.1	1.9	520 (8)	–	–	7	–	–	–	Stable.
B-1364	1.088	2.398	3.050	0.0753	501.7	72.77	1580.1	5184	89.2	11.0	1.6	–	–	65 (1)	6	–	–	–	Stable.
B-1365	1.096	2.417	3.083	0.0743	502.7	72.91	1570.6	5153	88.9	11.0	1.6	–	–	130 (2)	6	–	–	–	Stable.
B-1366	1.151	2.537	2.996	0.0806	530.4	76.93	1578.9	5180	88.9	13.1	1.9	–	–	260 (4)	7	–	–	–	Stable.
B-1367	1.071	2.362	3.607	0.0757	482.4	69.97	1542.6	5061	89.8	15.2	2.2	130 (2)	–	130 (2)	5/5	–	–	–	Stable.
B-1368	1.100	2.425	2.702	0.0755	515.3	74.73	1604.5	5264	88.8	9.7	1.4	130 (2)	–	–	6	–	–	–	Stable.
B-1369	1.053	2.322	1.944	0.0762	505.7	73.34	1644.7	5396	87.4	9.0	1.3	130 (2)	–	–	61	655	95	5270 to 5640	Stable but long damp time.
B-1370	1.101	2.427	2.967	0.0470	531.5	77.09	1653.8	5426	93.0	1.4	0.2	130 (2)	–	130 (2)[c]	6/4	–	–	–	Stable.
B-1371	1.088	2.399	3.010	0.105	473.9	68.73	1491.4	4893	84.1	20.7	3.0	130 (2)	–	–	6	–	–	–	Stable.
B-1372	0.771	1.699	3.052	0.0749	351.4	50.96	1561.5	5123	~88.9[d]	6.2	0.9	130 (2)	–	130 (2)	–	–	–	–	Stable. Damp time not obtained (tape recorder failed).
B-1373	1.354	2.985	2.989	0.0755	626.8	90.91	1585.6	5202	~89.1[d]	14.5	2.1	–	–	130 (2)	6	–	–	–	Stable.
B-1374	1.075	2.370	3.072	0.0751	499.7	72.47	1592.0	5223	90.1	21.4	3.1	130 (2)	130 (2)	130 (2)	10/9/7	–	–	–	Stable. 30.5 cm (12 in.) chamber.
B-1375	1.057	2.330	3.153	0.0737	491.0	71.21	1591.4	5221	90.5	–	–	130 (2)	–	–	6	–	–	–	Stable 17.8 cm (7 in.) chamber.
B-1376[a]	1.078	2.376	3.267	0.0732	498.5	72.30	1584.7	5199	90.6	19.3	2.8	–	–	–	–	–	–	–	Stable. No bomb used.

[a]Design chamber length except runs B-1374 and B-1375. Flow and performance data for ~1.8 s after ignition, except runs B-1351 through B-1356 (250–600 ms), B-1359 (800 ms), and B-1376 (1.3 s).

[b]Bomb fired during ignition transient before significant p_c rise.

[c]Reduced pulse amplitudes suggest only detonator fired.

[d]Value for $c_{t_A}^*$ based on linear interpolation between values for 551 and 689 kN/m² (80 and 100 psia) chamber pressure.

Table 4. Results for FLOX/B_2H_6 firings[a]

Run	$\dot{m}_t$ kg/s	$\dot{m}_t$ lbm/s	O/F	Z_t	$[p_{ce}]_t$ kN/m²	$[p_{ce}]_t$ psia	c^*_t m/s	c^*_t ft/s	η_{c^*}, %	p_c rms kN/m²	p_c rms psi	Bomb size, mg (grain)	Damp time, ms	Resonance: Amplitude kN/m²	Resonance: Amplitude psi	Resonance: Frequency, Hz	Start transient: Oxidizer-rich	Start transient: Fuel-rich	Remarks
																			Without cavities
C-343	1.158	2.552	2.814	0.112	684.9	99.34	2026.6	6649	94.4	2.1	0.3	130 (2)	4	–	–	–	X		Stable.
C-345	1.150	2.536	3.179	0.102	690.0	100.07	2054.7	6741	95.0	2.1	0.3	130 (2)	5	–	–	–	X		Stable.
C-346	1.139	2.511	3.182	0.0748	706.3	102.44	2123.8	6968	98.2	2.8	0.4	–	–	–	–	–	X		Stable. No bomb used.
C-347	0.933	2.056	2.105	0.101	575.0	83.39	2111.3	6927	100.8	1.4	0.2	–	–	–	–	–	X		Stable. No bomb used.
C-348	1.187	2.617	3.344	0.0700	725.6	105.23	2093.4	6868	96.4	2.8	0.4	130 (2)	3	–	–	–	X		Stable.
C-349	1.149	2.534	3.260	0.0735	706.3	102.44	2104.9	6906	97.2	2.1	0.3	130 (2)	3	–	–	–	X		Stable.
C-350	0.576	1.270	3.439	0.0705	341.9	49.59	2033.9	6673	93.5[b]	0.7	0.1	130 (2)	3	–	–	–	X		Stable.
C-351	1.092	2.408	3.149	0.0524	677.7	98.29	2125.7	6974	98.3	2.1	0.3	130 (2)	5	–	–	–	X		Stable.
C-352[a]	1.198	2.641	3.373	0.098	687.0	99.64	–	–	–	2.8	0.4	–	–	–	–	–		X	Stable. Run duration too short for performance.
C-354[a]	1.160	2.557	3.411	0.071	681.7	98.87	–	–	–	2.8	0.4	130 (2)[c]	30	–	–	–		X	Stable but long damp time.
C-344[a]	1.084	2.389	5.248	0.069	419.4	60.82	–	–	–	–	–	130 (2)	–	1241	180	6080		X	Unstable spontaneously during start (before bomb).
C-353[a]	1.194	2.633	3.052	0.105	635.2	92.12	–	–	–	–	–	130 (2)	–	1517	220	6400 to 6510		X	Unstable spontaneously during start (before bomb).
																			With cavities
C-340	1.127	2.485	3.298	0.0725	701.5	101.74	2132.1	6995	98.4	2.1	0.3	–	–	–	–	–	X		Stable. No bomb used.
C-341	1.174	2.589	2.763	0.113	710.9	103.10	2073.6	6803	96.7	2.1	0.3	–	–	–	–	–	X		Stable. No bomb used.
C-342	1.197	2.638	2.761	0.113	724.9	105.14	2075.1	6808	96.8	2.1	0.3	130 (2)	3	–	–	–	X		Stable.
C-355	1.114	2.455	3.100	0.0762	676.9	98.17	2082.1	6831	96.3	1.4	0.2	130 (2)	5	–	–	–		X	Stable.
C-356	1.154	2.543	3.050	0.105	697.8	101.20	2072.0	6798	96.0	1.4	0.2	130 (2)[c]	20	–	–	–		X	Stable but long damp time.
C-357	1.129	2.490	3.034	0.106	673.9	97.74	2043.4	6704	94.7	1.4	0.2	130 (2)	5	–	–	–		X	Stable. Cavity height reduced to 1.5 mm (0.07 in.).
C-358[a]	1.042	2.297	2.693	0.116	648.8	94.09	–	–	–	–	–	–	–	1241	180	6350		X	Unstable spontaneously during start. Cavity length reduced to 10.9 mm (0.43 in.).

[a]All runs made with design chamber length. Flow and performance data for ~2.4 s after ignition except C-352 and C-354 (both ~600 ms), C-344 (190 ms), C-353 (370 ms), and C-358 (280 ms).

[b]Value for $c^*_{t_h}$ based on value for 689 kN/m² (100 psia) chamber pressure.

[c]Bomb fired during starting transient, but after ignition and significant p_c rise.

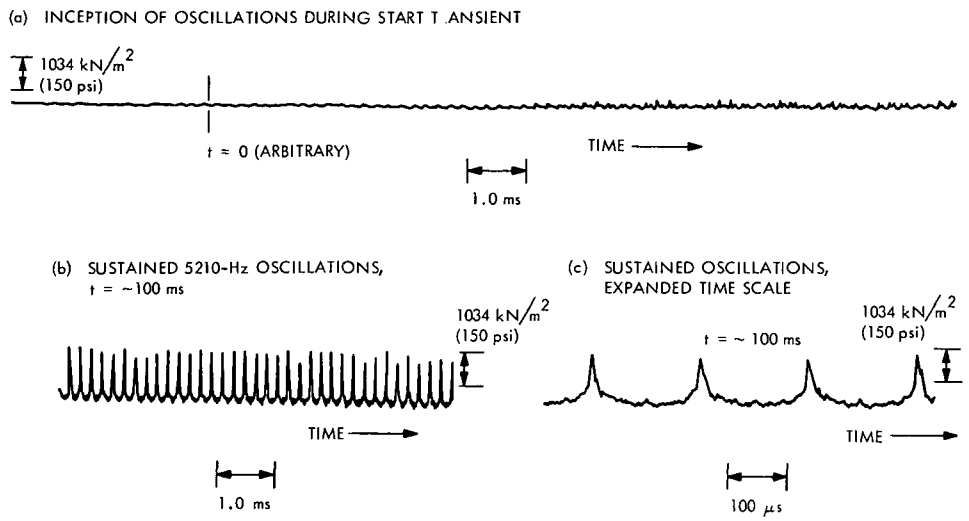

Fig. 5. Typical experimentally observed resonance, O_2/C_2H_4, without cavities (run B-1353)

3. Cavity gas temperature. Cavity gas temperature measurements during all firings were well below the design value of 990 K. Representative values of these measurements are difficult to designate because they varied considerably during individual firings as well as for different firings. The fact that measurements made for diametrically opposed cavities differed consistently by about a factor of 2 indicated that gross circumferential differences also existed. Thus, an overall temperature range for all firings of from 331 to 513 K (135 to 464°F) was observed at an arbitrary constant time of 1.8 s after main flow ignition. For most of the firings, the temperatures appeared to approach a stable value at this time.

4. Performance. Steady-state performance of the combustor (uncorrected for any losses) for the stable firings with O_2/C_2H_4 is summarized in Fig. 6 in terms of characteristic velocity (c^*), c^* efficiency ($\eta_{c*} = c^* \exp/c^*_{th}$), and combustion roughness (p_c rms) versus mixture ratio (O/F) and barrier mass fraction (Z_t). Description and definition of all variables are contained in Appendix B.

Characteristic velocity data presented in Fig. 6 are based on chamber pressure measurements at the head end (injector face) of the chamber. Analogous data based on pressure measurements at the nozzle entrance were consistently 3–4% higher, this difference being observed even though the static pressures for both locations were converted to throat stagnation pressure as described in Appendix B. Past JPL experience has indicated that the difference is related primarily to the simplifying assumptions of one-dimensional, constant gas property flow in the standard procedures of converting static pressures to nozzle stagnation pressure–where, in fact, the real combustion processes encompass multidimensional flow, incomplete energy release prior to the nozzle throat, and nonuniform gas properties. Thus, the choice of which value for c^* is the more correct is not obvious, although the justification of a choice can be improved if accurate thrust measurements are also available. Since thrust was not measured here, no such justification will be made.

On a relative basis, it can be seen from Fig. 6 that:

(1) η_{c*} increased somewhat with increasing O/F.

(2) η_{c*} decreased rapidly with increasing Z_t.

(3) η_{c*} was not significantly modified by either combustor length or combustion pressure level.

(4) Combustion roughness tended to increase with both increasing O/F and increasing Z_t. A value of ~13.8 kN/m² (2 psi) rms was obtained for near-design flow conditions.

B. FLOX/B_2H_6 (Design Propellants)

A total of 19 firings were conducted using the FLOX/B_2H_6 propellants. Twelve firings were made without the damping cavities. The remaining seven were made with damping cavities installed–five with the design configuration and two with modified cavities. Results are summarized in Table 4.

1. Firings without cavities. Two of the firings without cavities were spontaneously unstable, with transitions to sustained resonance occurring essentially at the time of

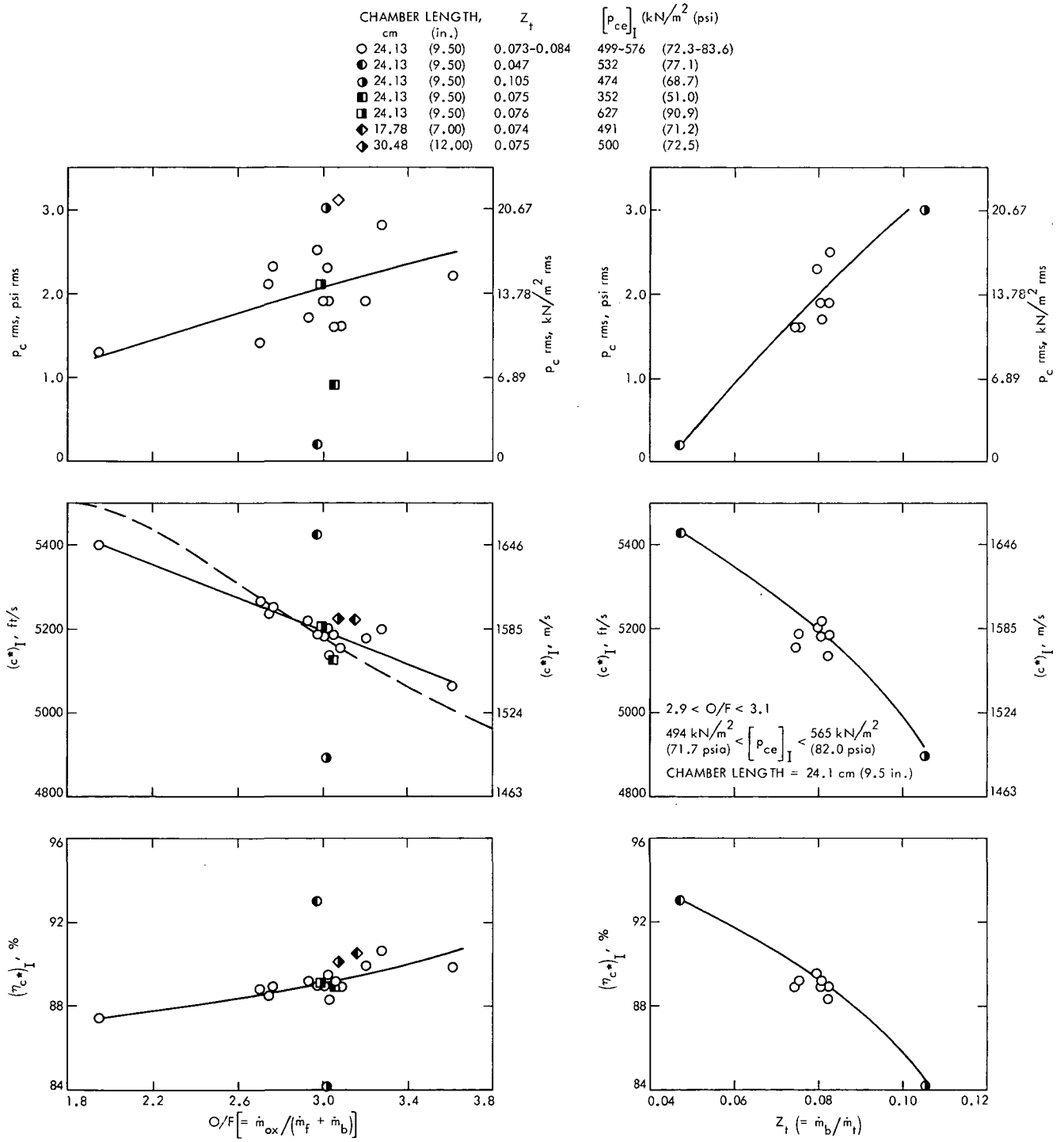

Fig. 6. Experimental performance of OF_2/B_2H_6 engine using O_2/C_2H_4. All data for runs with cavities.

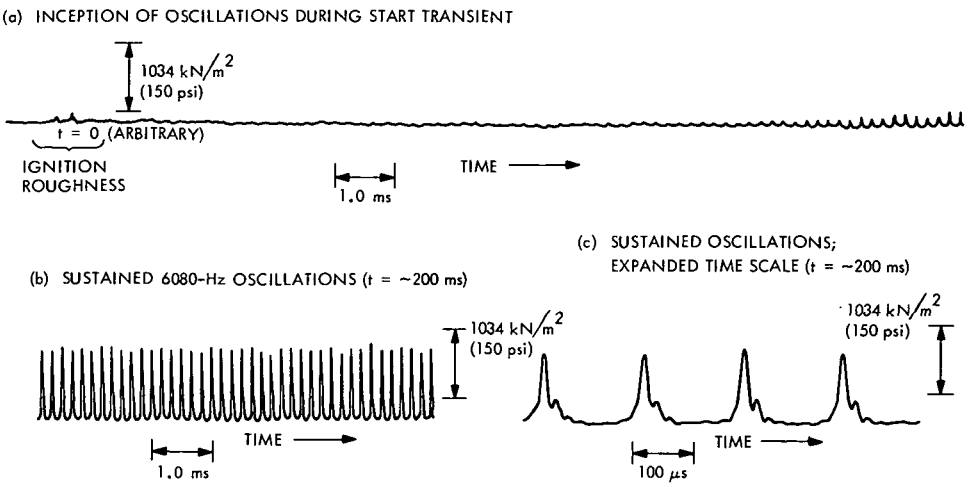

Fig. 7. Typical experimentally observed resonance, FLOX/B_2H_6, without cavities (run C-344)

ignition. Although the growth of initially small oscillations to a nonlinear spinning wave was similar to that observed with O_2/C_2H_4, the hypergolic ignition process with the FLOX/B_2H_6 was rough under some conditions, and the roughness evidently precipitated the initial oscillations. Ignition roughness was accentuated whenever fuel-rich starts were present; however, only two of the four starts under this condition were unstable. All eight starts under oxidizer-rich ignition conditions were stable. An example of the precipitation of resonance and the character of the sustained first tangential traveling wave is shown in Fig. 7. Comparison of these resonance characteristics with those for O_2/C_2H_4 (Fig. 5) reveals substantially the same behavior except for the expected greater frequency with the hotter FLOX/B_2H_6 combustion gases.

Five of the ten stable firings (without cavities) were also perturbed with 130-mg (2-grain) bombs detonated either during midfiring (four runs) or the starting transient (one run). Pulse amplitudes of 689 kN/m² (100 psi) or greater were observed, which were damped in 5 ms or less (Fig. 8b), except for the firing with the bomb-pulsed start, which exhibited a 30-ms damping time.

2. Firings with design cavities. As with the O_2/C_2H_4 firings, the installation of the design damping cavities apparently stabilized the combustor. Two firings were conducted with fuel-rich ignition and three with 130-mg (2-grain) bombs. All five firings were stable. One of the firings had both a fuel-rich and a bomb-pulsed start. The ignition transient of that run precipitated a low-amplitude (~40 kN/m² or 6 psi) oscillation of ~5500 Hz that persisted for ~90 ms while the bomb pulse, which occurred after the decay of the ignition oscillation, exhibited a 20-ms damping time. The other firings, bombed at midrun, exhibited the same short (<5 ms) damping times as the firings without cavities (Fig. 8c). The three firings with oxidizer-rich ignition were stable.

3. Start transient oscillations. Although the ignition-precipitated oscillations noted above were of somewhat greater amplitude than typical, nearly all of the stable firings with FLOX/B_2H_6 exhibited small-amplitude (7–30 kN/m² or 1–4 psi) high-frequency oscillations (5000–5500 Hz) for periods of 50 to 200 ms during the starts, regardless of ignition mixture ratio or the presence of cavities. Also, nearly all starts under oxidizer-rich conditions exhibited a "buzz" frequency of from 450 to 520 Hz for periods of from 50 to 100 ms with maximum amplitudes ranging from 14 to 100 kN/m² (2 to 14 psi). A more quantitative correlation of the observed dynamic behavior of the combustor with the starting mixture ratio transient than given here is probably not possible because of the question of nitrogen purge gas diluent mentioned previously in Section IV. Suffice it to say that the FLOX/B_2H_6 starting transient, as for the O_2/C_2H_4 starting transient, was the precipitative agent for sustained resonance when the additional damping from cavities was absent.

4. Off-design cavity dimensions. Ultimately the cavity dimensions were altered from the design configuration in a cursory attempt to simulate the effects of solids deposition. Two firings were made with cavity alterations. In the first, only the cavity width was changed from the 3.3-mm (0.13-in.) design value to 1.5 mm (0.07 in.). This cavity size was tested with a fuel-rich start and a midrun bomb pulse (130 mg or 2 grains). The firing was stable with a

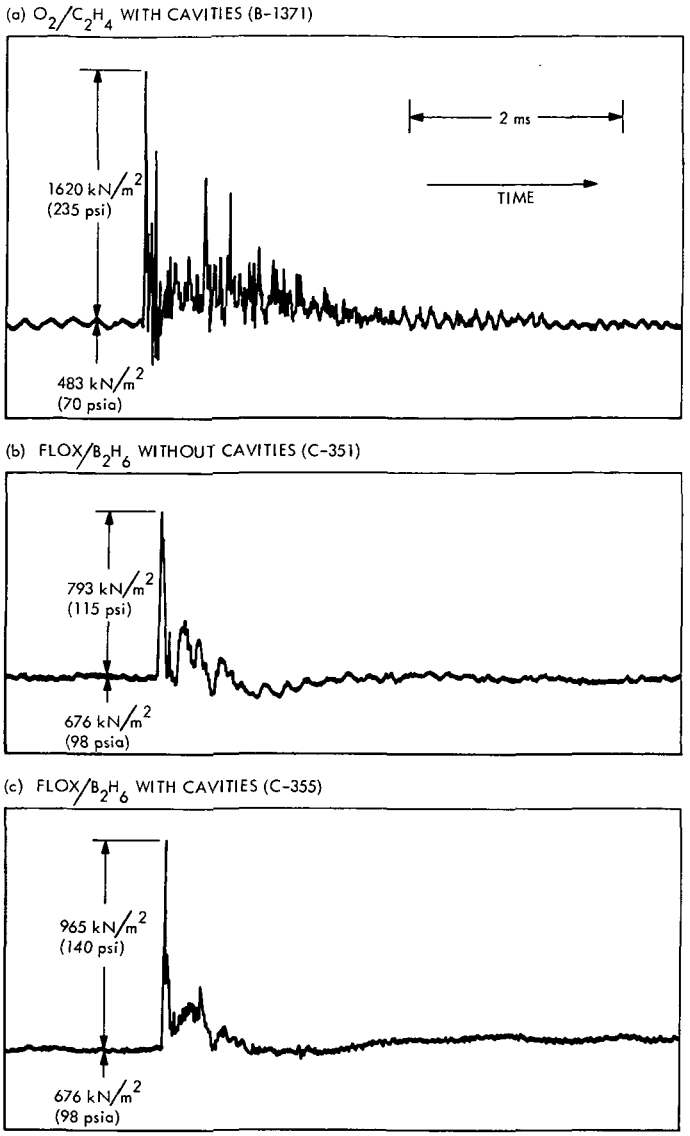

Fig. 8. Typical bomb pulses (130 mg or 2 grains), measured with Kistler transducers located 1.27 cm (0.5 in.) from injector face

pulse damping time of 5 ms and essentially no starting transient oscillations. The second alteration changed only the cavity depth from the 21.8-mm (0.86-in.) design value to 10.9 mm (0.43 in.). In the test firing, a fuel-rich start precipitated a sustained spinning wave, essentially identical to that shown in Fig. 7 for no cavities. Thus, the reduced depth is apparently the more detrimental change to cavity effectiveness.

5. Cavity gas temperatures. Cavity gas temperatures were again taken during three of the firings with the design cavity dimensions. And again the gas temperatures were well below the design value. While perhaps not as great as for the O_2/C_2H_4 firings, the same kind of variations were observed; i.e., circumferential and sporadic variations during the firings as well as for different firings. The observed temperatures for this run series ranged from 339 to 470 K (150–386°F) at a constant time of 1.8 s from ignition, where they appeared to approach a stabilized value during most firings.

6. Performance. The performance characteristics of the stable FLOX/B_2H_6 firings, obtained in the same manner as for the O_2/C_2H_4 firings, are summarized in Fig. 9. These data show that for FLOX/B_2H_6:

(1) η_{c*} tended to decrease slightly with increasing O/F, a trend contrary to the data for O_2/C_2H_4.

(2) η_{c*} decreased with increasing Z_t.

(3) Reduced combustion pressure may decrease η_{c*} somewhat; however, that observation is based on only one firing, which was inadvertently made at a considerably off-design mixture ratio.

(4) Combustion roughness was nearly constant at ~2.1 kN/m^2 (0.3 psi) rms for all flow conditions tested. Thus stable FLOX/B_2H_6 combustion was significantly smoother than for O_2/C_2H_4. Also note that the presence of the cavities did not significantly reduce the level of combustion noise.

7. Solids deposition. Significant amounts of solids deposition were encountered throughout the FLOX/B_2H_6 firing series. The typical appearance of the internal surfaces of the combustor after a single firing (all hardware was cleaned before each firing) is shown in Fig. 10.

Figure 10a shows the injector region of the combustor, including the entrance areas of the damping cavities where at least some blockage of the entrances is apparent. Figure 10b shows a different view of the injector face with the chamber section removed. The nonuniform thickness of deposition, particularly near the orifices, is apparent in both Fig. 10a and 10b. The rather uniform deposition on the internal surfaces of the cavities is shown in Figs. 10b, c, and d, where a coating estimated to be as much as 0.5 mm (~0.020 in.) thick was observed.

Whether these deposits occurred during starting or termination transients, or during the firing, was not determined; however, examination of the chamber before cleaning (between firings) revealed little difference in appearance between 0.5-s and 2.5-s duration firings. The

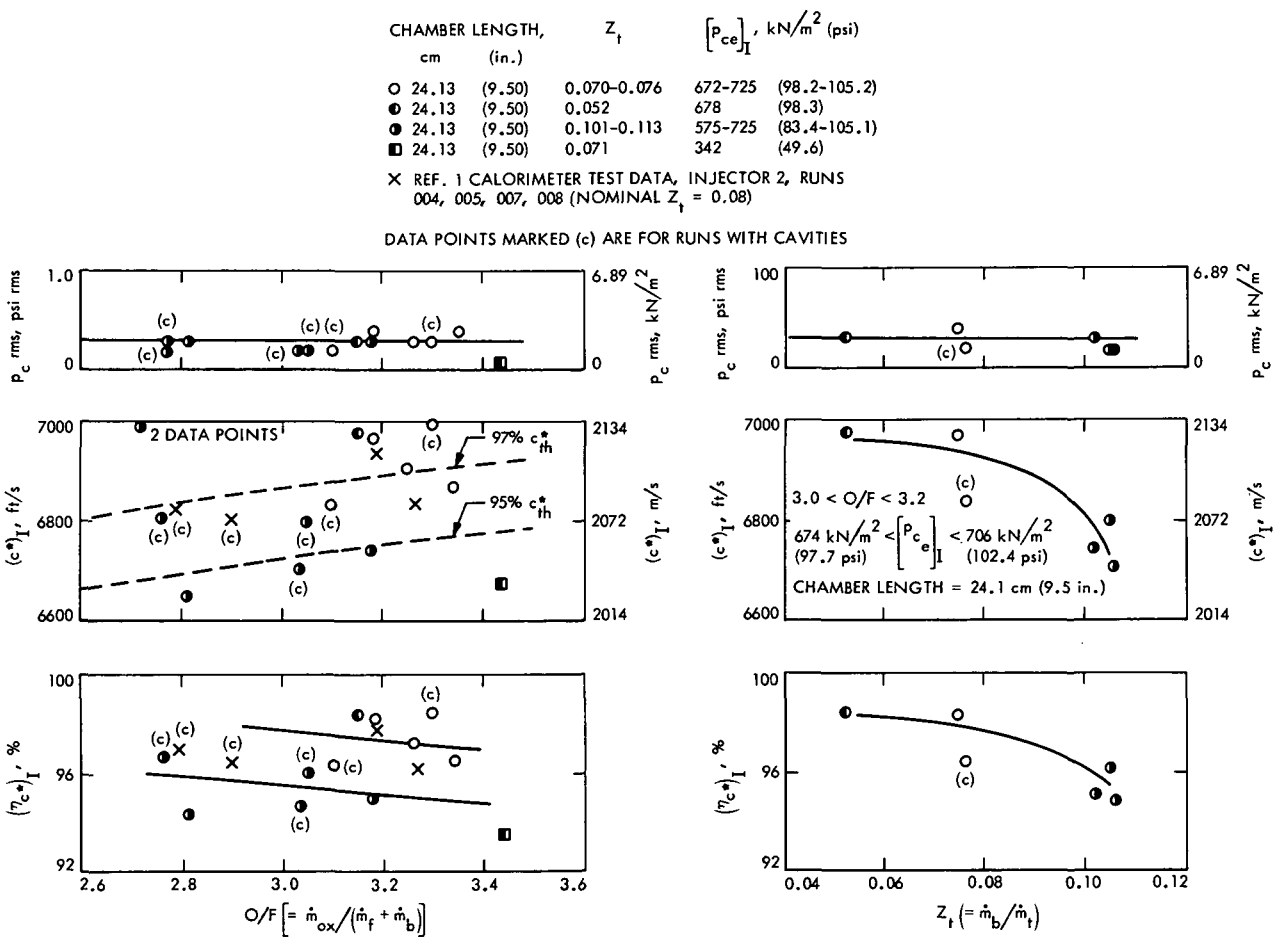

Fig. 9. Experimental performance of OF_2/B_2H_6 engine using FLOX/B_2H_6

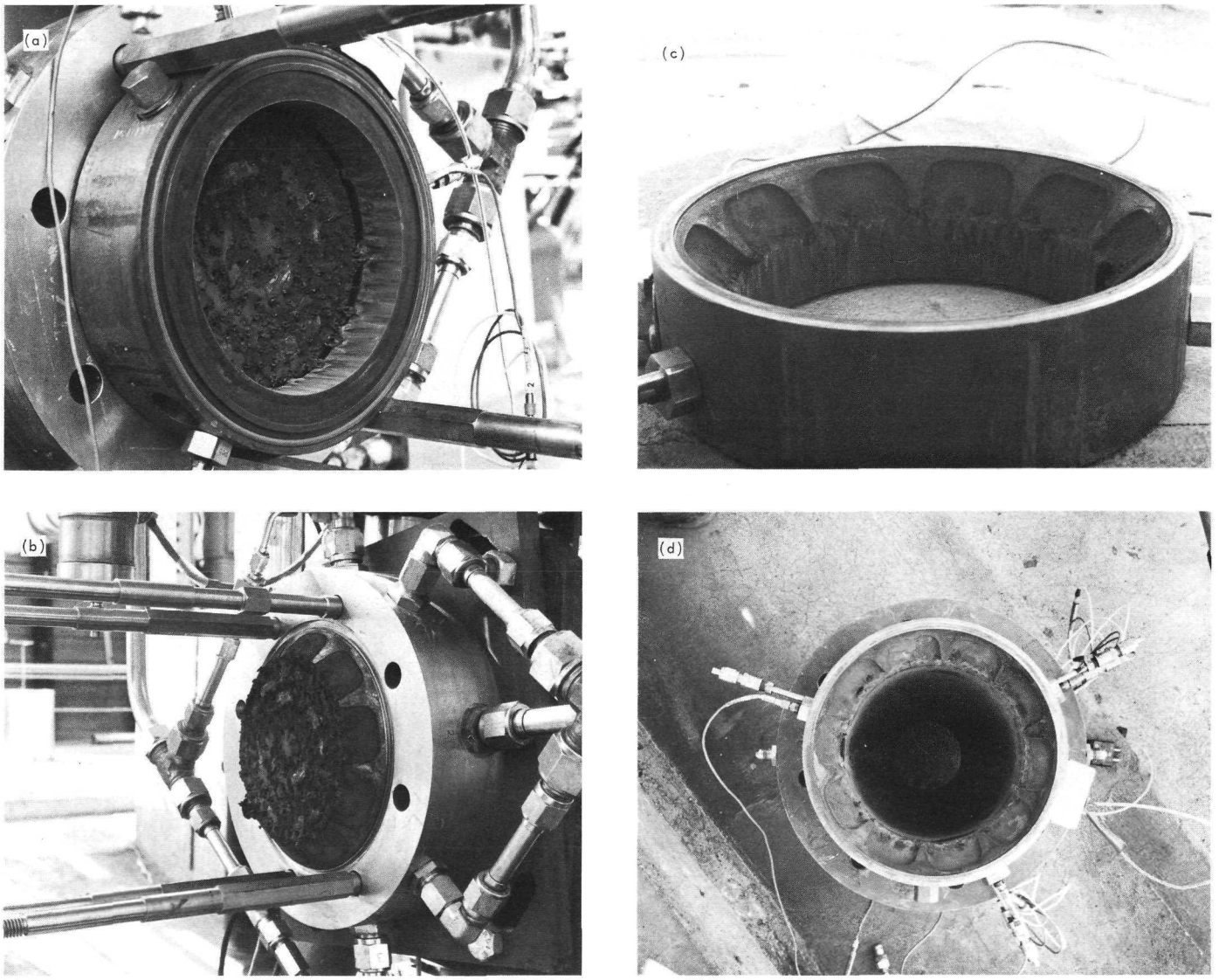

Fig. 10. Typical solids deposition with FLOX/B_2H_6 (run C-342): (a) injector and cavity entrance region, (b) injector face and cavity surfaces, (c) cavity surfaces, side view, and (d) cavity surfaces, top view

composition of the deposits was not determined by analysis, since it closely resembled samples of material deposited in other (liquid–liquid FLOX/B_2H_6 combustion) engines for which chemical analysis had shown the material to be largely B_2O_3 and elemental B (Ref. 7). The material was easily removed with a soft bristle brush and a water flush, a result that was also consistent with previous experience.

VI. Discussion

A. Insensitivity to Bomb Disturbances

None of the bomb disturbances utilized in this evaluation initiated a sustained resonant mode even without the damping cavities. Yet the uninhibited combustor exhibited a low margin of stability to small disturbances originating during starting transients. This is in contrast to the usual sensitivity of an unstable liquid–liquid combustor to bomb pulse disturbances and leads one to speculate that perhaps the turbulent-mixing, controlled-energy release processes, as associated with this engine, are less sensitive to the blast-wave type of perturbation than to the more continuous gradients of spontaneously generated fluctuations. On the other hand, this generalization is not supported by the observation that, at least for the FLOX/B_2H_6 firings, even the spontaneous fluctuations were ineffective in precipitating resonance once quasi-steady-state conditions of flows and combustion pressure were achieved; e.g., no transitions to resonance were observed after completion of the starting transients even though combustion noise was always present. Thus, one is led to a more involved speculation that the combustor was sensitive to a particular combination of mixture ratio, low combustion pressure, and form of perturbation that was satisfied in these experiments only during the early phase of some starting transients.

The fact that the combustor exhibited a similar sensitivity to the starting transient with either propellant combination suggests that thermochemical differences between the two combinations were relatively unimportant to combustor stability. Therefore, the important mechanism coupling energy release with pressure oscillations in this combustor appears to be reactant mixedness and mixing dependence on local transverse (or tangential) gas motion, although some form of injected flow coupling cannot be conclusively ruled out. Evidently the bomb pulses used here did not produce an adequately coupled disturbance although the bomb-pulsed starting transients mentioned in Section V-B exhibited an unusually long damping time, and hence coupling conditions may nearly have been satisfied in those cases.

One explanation of the apparent low sensitivity of the gas–gas mixing controlled combustor to the blast wave discontinuity may lie in the fact that reduced peak concentrations of available energy exist in the chamber. This is true because no energy exists in the concentrated form of liquid streams or particles as in the case with liquid injection, where a finite time (and axial distance) is required for evaporation. Thus, a shock-fronted blast wave can release the energy of a spray field of mixed liquid droplets by reducing the spray to a micromist where very fast combustion can occur and enhance the coupling of the concentrated energy release with the traversing disturbance.

B. Cavity Damping Effectiveness

The design configuration for the damping cavities was highly effective in stabilizing the combustor; however, verification of their intended operation as quarter-wave acoustic devices by comparisons of the pressure oscillations at the open and closed ends of the cavities was not attempted. On the basis of acoustic theory (Refs. 8–10) such a verification would show that maximum damping is achieved when the cavity resonant frequency is equal to the chamber frequency. When that condition is sustained, the pressure oscillation at the closed end of the cavity lags the chamber pressure oscillation by $\pi/2$ rad (90 deg) and the ratio of closed to open end oscillatory pressure amplitude reaches a peak (> 1).

Of course adequate cavity effectiveness does not necessarily require that the cavities operate precisely at their resonant condition or even that they operate as classical acoustical devices at all, it only being necessary that they dissipate more energy than the net driving energy in the combustion chamber. The fact that the measured cavity gas temperatures were 50 to 70% below the design value suggests that the cavity resonant frequency was reduced by as much as 30 to 40%, a degree of detuning which would drastically reduce cavity damping on the basis of quarter-wave-tube theory, indeed almost eliminating damping. However, since the measured temperatures were located near the closed end of the cavities, a temperature gradient may have existed providing a somewhat higher effective gas temperature.

Interestingly enough, the damping times for bomb pulses imposed during midfirings, as well as combustion roughness, were essentially the same with or without cavities (FLOX/B_2H_6 firings, Table 4). This suggests that the damping attributable to the cavities under steady state

operating conditions was nil. However, their effectiveness for inhibiting the growth of the small amplitude oscillations during starting transients seems clear. Indeed, these starting transient oscillations were some 15 to 20% lower frequency (5000–5500 Hz) than the design chamber frequency (6200 Hz); therefore the cavities may have operated nearer resonance during the starting period. A similar argument could be made for the effectiveness of the cavities in the O_2/C_2H_4 firings, where even the fully developed chamber mode frequency was nominally 5500 Hz.

The cursory examination of the effect of reduced cavity dimensions (a simulation of solids deposits) made with $FLOX/B_2H_6$ propellants suggests that a 50% reduction of cavity open area in this combustor does not measurably reduce damping effectiveness. However, this is not well substantiated because the incidence of instability was not 100% even without the cavities. Nonetheless, from quarter-wave acoustic theory, that reduction of open area should have produced a significant reduction in damping through both increased cavity impedance and increased cavity resonant frequency.

Reducing the length of the cavities by 50% clearly destroyed their effectiveness, since a spinning wave of essentially the same amplitude as for the chamber with no cavities was developed and sustained. That length reduction would, of course, about double the cavity resonant frequency, assuming the gas properties were unchanged, and hence would reduce damping for the starting transient chamber oscillations as well as for the fully developed wave.

In summary, the design cavity configuration appears to have been most effective in damping chamber oscillations during the starting transients and essentially ineffective in providing additional damping for the bomb pulse oscillations. However, the combustor response to the starting transient perturbations was high, while being essentially nil to the bomb pulses; therefore, the cavities were effective in stabilizing the engine. Elucidation of the main dissipative mechanism provided by the cavities cannot be made from the data obtained, but the results imply that the cavities operated considerably off-resonance on the basis of quarter-wave cavity acoustic theory. Thus, a substantial amount of cavity damping action may occur through mechanisms not dependent on classic acoustic relationships between the chamber and the cavities. One such mechanism may be a relatively simple venting or relieving effect which would serve to decouple the combustion energy release at the chamber/injector juncture where tangential mode oscillations are most intense.

C. Comparison of Results

Since the combustor evaluated in these experiments functionally duplicated an existing engine[8] that has undergone independent heavyweight chamber tests (Ref. 1) as well as regeneratively cooled tests of longer duration, it is of interest to compare some of the results. Such a comparison serves to indicate some aspects of reproducibility of the combustor design.

1. Stability. While the comparable engine has not undergone bombing tests, that engine has exhibited one spontaneously unstable firing when the combustor was operated without cavities and with an above-design barrier flow rate (Ref. 1). Details of the resonant mode that was precipitated during the starting transient are not available; however, the sustained resonance damaged the injector face and thus was probably a tangential mode of relatively high amplitude. Subsequent longer-duration firings with the design cavities installed and with a regeneratively cooled chamber have been stable. These results are consistent with the results reported herein.

2. Performance. Characteristic velocity performance (uncorrected for losses) reported in Ref. 1 for a series of short-duration tests with a heavyweight chamber are shown as the $\times$ data points in Fig. 9. Performance appears to have been reproducible within $\pm 1\%$.

3. Solids deposits. This characteristic seems to be inconsistent. For the experiments reported herein, significant amounts of deposits were found in the shortest runs. However, the results reported in Ref. 1 show very small deposits even for long-duration firings of up to 50 s. Since the two combustors were essentially duplicates and since the measured steady state performances were nearly the same, the difference in solids accumulation may reflect differences in starting or termination transients. A quantitative evaluation of the effects of these transients on solids deposition could not be made with the feed system used in the JPL experiments, but it is believed that these effects should be evaluated further. For instance, the deposition of significant quantities of solids in the damping cavities, even if only during transient conditions, could be accumulative for multiple firings, potentially rendering the cavities ineffective.

[8]Utilizing the so-called unit No. 2 injector of Contract NAS7-765.

VII. Conclusions

The following conclusions have been drawn:

(1) The gas–gas OF_2/B_2H_6 combustor utilizing FLOX/B_2H_6 (70–30 FLOX being a simulant for OF_2) or O_2/C_2H_4 is unstable when it is not equipped with supplemental damping cavities.

(2) Without cavities, the combustor response to starting transient perturbations is sufficient to precipitate sustained combustor resonance (first tangential spinning mode) for either propellant combination. For the FLOX/B_2H_6, this response is greatest under fuel-rich starting transients.

(3) Combustor response (using FLOX/B_2H_6) to the bomb disturbances as used in these experiments is insufficient to precipitate sustained resonance with or without cavities.

(4) The design cavity configuration, based on a quarter-wave acoustic damping concept, provides sufficient damping to stabilize the engine to the starting transient perturbations. Their damping contribution to bomb pulses under steady-state operating conditions is negligible since damping times are the same with and without the cavities.

(5) Since the cavities appear to be operating sufficiently off-tune to seriously degrade their damping as predicted by quarter-wave acoustic theory, a substantial contribution to their dissipative action may occur through nonacoustic mechanisms such as energy release decoupling effects at the corner of the chamber.

(6) Solid deposits would degrade cavity effectiveness, especially if the deposits reduced the depth of the cavity.

(7) Performance and stability characteristics from the JPL experiments are consistent with limited results for an independently tested duplicate engine. However, contrary solids deposition characteristics are obtained, where significant amounts are observed in the JPL experiments. A significant factor in solids deposition may be starting and termination transients.

Nomenclature

A flow area

A'_i virial coefficients,[9] $i = 1, 2, 4, 5$

B_i constants for specific gases in virial coefficient[9] A'_1, $i = 0, 1, 3, 5$

C_i constants for specific gases in virial coefficient[9] A'_2, $i = 0, 1, j$, or variables in virial coefficient A'_2, $i = 3, 5$

C'_i constants for specific gases in virial coefficients[9] A'_2 and A'_4, $i = 3, 5$

C''_3 constant for specific gas in virial coefficients[9] A'_2 and A'_4

E_1 constant for specific gas in virial coefficient[9] A'_5

C_d venturi discharge coefficient, actual flow rate/ideal flow rate

c^* experimental characteristic velocity, defined by Eq. (B-16)

c^*_{th} theoretical characteristic velocity, based on one-dimensional equilibrium considerations

D venturi inlet diameter

d venturi throat diameter

g_c gravitational conversion factor in general relationship: force = mass × acceleration/g_c

h enthalpy per unit mass

h_0 ideal-gas enthalpy per unit mass

K_i polynomial coefficients in Eq. (B-8) obtained by curve fitting, $i = 0, 1, 2, 3$

$K_{I,N}$ stagnation pressure conversion factors, defined under Eq. (B-15)

M chamber flow Mach number

$\dot{m}$ mass flow rate, defined in Eqs. (B-1) and (B-12)

O/F mixture ratio, defined in Eq. (B-13)

P_R reduced pressure, pressure/critical pressure of specific gas

P' pressure normalized by atmospheric pressure

p absolute pressure

p_c static chamber pressure (measured)

p_{ce} isentropic nozzle-throat stagnation pressure, defined in Eq. (B-15)

p_c rms electronically generated measure of combustion roughness, described in Appendix B

R specific gas constant, universal gas constant/molecular weight

S entropy per unit mass

S_0 ideal-gas entropy per unit mass

t time

T absolute temperature

T_R reduced temperature, temperature/critical temperature

Z_t barrier fuel mass fraction, defined in Eq. (B-14)

Z' compressibility factor, defined in Eq. (B-4)

γ specific heat ratio

η_{c^*} c^* efficiency, defined in Eq. (B-17)

ρ mass density

ρ_R reduced density, density/critical density

Subscripts

2 venturi stations downstream of inlet station

b barrier fuel

f core fuel

ox oxidizer

t total

thr nozzle throat

v venturi inlet station

x assigned reference station between venturi inlet and throat

I injector end of chamber

N nozzle entrance end of chamber

Superscripts

* sonic station in venturi

[9]Symbols A'_i through E_1 are defined following Eq. (B-6).

Appendix A

Pulsing Device

Design of the pulsing device (bomb) used in this evaluation evolved from a similar device used in previous JPL combustion stability research (see Ref. 4). In the previous work, experience had shown that the older bomb assembly, utilizing standard electrically detonated blasting caps with metallic cases, produced shrapnel that was damaging to the interior surfaces of the combustor. Also, only a few charge strengths were commercially available, especially for charge sizes less than 130 mg (2 grains). Since it was obviously desirable to avoid shrapnel damage and since small charge sizes were desired for the relatively small OF_2/B_2H_6 combustor, a new bomb assembly was devised.

The new assembly underwent a certain evolution of its details as it was used; however, the conceptual design remained the same and is shown schematically in Fig. A-1. A view of its installation in the chamber section nearest to the face is shown in Fig. A-2.

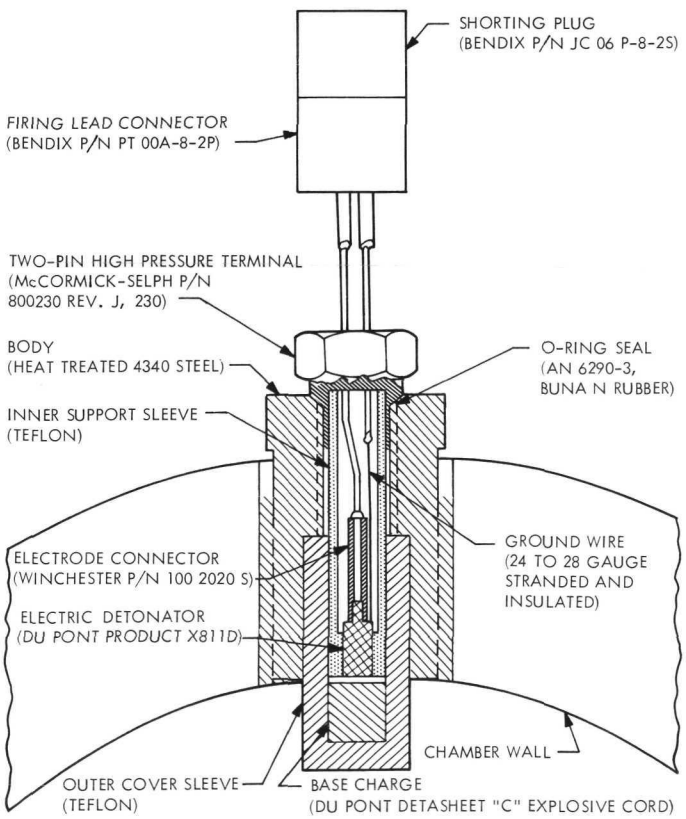

Fig. A-1. Schematic of pulsing device (bomb)

The assembly consists of an electrically initiated miniature detonator (du Pont[10] product number X-811D); a base charge (du Pont Detasheet "C" explosive cord, 63% by weight PETN); a Teflon outer cover sleeve for thermal

[10]Chemical Products Sales Division—Explosives Department, E. I. du Pont de Nemours & Co., Inc., Wilmington, Del.

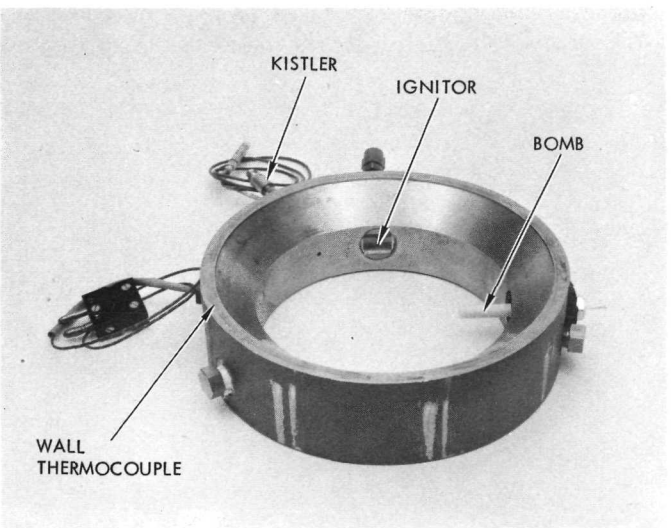

Fig. A-2. View of chamber section nearest to injector (without cavities)

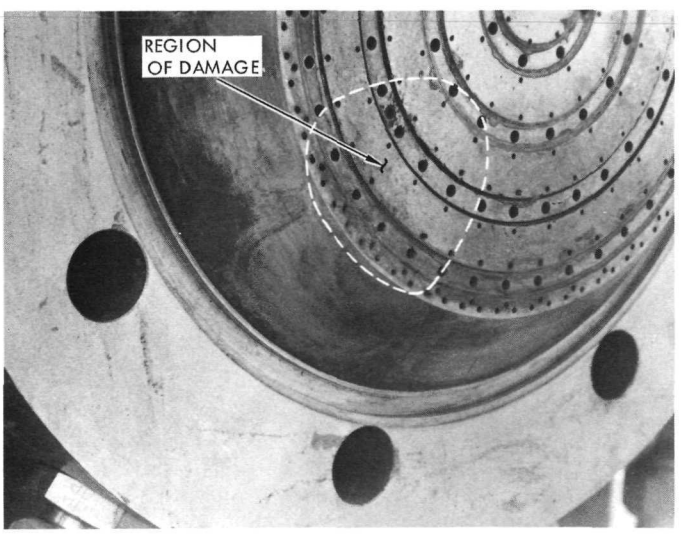

Fig. A-3. View of accumulated damage to injector face from bomb fragmentation (after run C-342)

isolation; and miscellaneous mechanical support and electrical connection elements.

Nominal bomb sizes mentioned in this report neglect the detonator charge (~50 mg) and refer only to the base charge size, controlled during bomb assembly by the length of the installed explosive cord.

Based on data from Ref. 11, a 1.14-mm (0.045-in.) thick cover sleeve was initially used, but that was found to be completely inadequate for the ~1-s exposure time desired. Ultimately the wall thickness was increased to 3.05 mm (0.12 in.), which still provided reliable operation only for bombs placed near the injector.

Damage from shrapnel was reduced with the new configuration by excluding metallic materials from the area of the base charge and by confining the metallic-encased detonator within the body of the assembly. However, localized pitting of the injector face was still noted, apparently as the result of high-velocity particles of Teflon. Figure A-3 shows the appearance of the accumulated damage after 14 tests with bombs ranging from 65 to 520 mg (1 to 8 grains) located 1.27 cm (0.5 in.) from the face. Although this damage would be objectionable for flight-rated components, it is not considered to have influenced the stability evaluation.

Appendix B

Measurements and Data Reduction

I. Venturis and Calibrations

Sonic venturi flowmeters having the characteristic dimensions illustrated in Fig. B-1 were used throughout the evaluation. As is well known, flow rates can be deduced with these devices from measurements of total pressure and temperature at the entrance to the venturi, using known calibration factors and fluid properties and following appropriate computational procedures.

In the present case, all venturis were designed with a large enough entrance contraction area ratio ($\sim$20) that the difference between total and static properties was negligible ($<$0.04%); therefore, averaged redundant, static values of pressure and temperature were used.

Discharge coefficients (C_d) were determined by means of calibrations with gaseous N_2. For these calibrations, the venturi was located in the N_2 pressurant line supplying a tank from which water was displaced (by the N_2) through an accurately calibrated turbine flowmeter. Using the volumetric flow rate indicated by the turbine meter as the standard and the state properties of the N_2 in the tank ullage space deduced from pressure and temperature measurements, the mass flow rate of N_2 through the venturi was determined. The venturi C_d was then computed using the standard definition, C_d = actual flow rate/ideal flow rate, where the ideal flow rate is for the measured venturi inlet pressure and temperature. A constant value of $C_d = 0.992$ was established for the flow range of interest for all venturis.

	d		D	
	cm	(in.)	cm	(in.)
OXIDIZER	1.212	(0.478)	5.860	(2.31)
CORE FUEL	0.660	(0.260)	3.560	(1.402)
BARRIER FUEL[a]				
B	0.450	(0.177)	2.290	(0.902)
B_1	0.348	(0.137)	2.340	(0.922)
B_2	0.445	(0.175)	2.340	(0.922)
B_3	0.570	(0.224)	2.340	(0.922)

[a]FOUR DIFFERENT BARRIER FUEL VENTURIS USED.

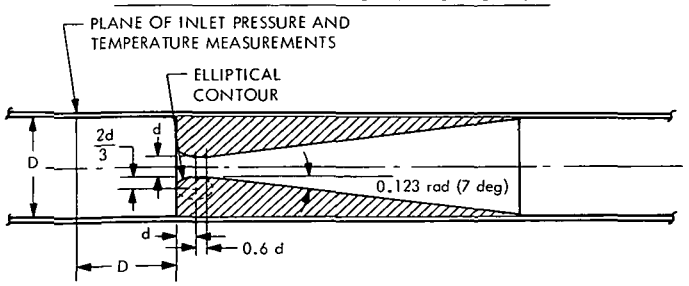

Fig. B-1. Sonic venturi configurations

The ideal N_2 flow rates were computed by both methods described below, with an average difference between methods of 0.2% for the 15 calibration runs, indicating that real gas effects in the expansion process between venturi inlet and throat were negligible for the N_2. This agreement in flow computation lends credence to the computational procedure (below) for real gas effects and also indicates that the standard sonic venturi equation is adequate for O_2 and FLOX gas flow computations within the 0.2% order of accuracy.

II. Oxidizer Flow Rate Computation

The following relationship based on the standard sonic venturi equation was used for calculating O_2 and FLOX flow rates (using appropriate units):

$$m = \frac{A^* p_v C_d}{Z_v' T_v}\left[\frac{g_c \gamma}{R}\left(\frac{2}{\gamma+1}\right)^{(\gamma+1)/(\gamma-1)}\right]^{1/2} \quad \text{(B-1)}$$

where

m = mass flow rate

A^* = venturi throat area

p_v = venturi inlet total absolute pressure

T_v = venturi inlet total absolute temperature

Z_v' = compressibility factor, a function of p_v and T_v

C_d = discharge coefficient

g_c = gravitational conversion factor in general relationship: force = quantity of matter $\times$ acceleration/g_c

R = specific gas constant

γ = ratio of specific heats, a function of p_v and T_v

Gas properties from Ref. 12–14 were used for O_2, N_2, and 70-30% FLOX.

III. Fuel Flow Rate Computation

Both C_2H_4 and B_2H_6 gases are subject to significant variations in specific heats and compressibility factors over the range of temperature and pressure changes associated with expansion from the inlet to the throat of the venturi. Those effects were found to produce errors of as much as 10 to 20% if the standard venturi equation was used. The technique outlined in Ref. 15 was ultimately adapted for circumventing this difficulty.

Basically the problem is to establish the enthalpy and density at the sonic throat, accounting for the variations noted above as the gas expands via an assumed one-dimensional, isentropic process from the measured inlet pressure and temperature to sonic conditions. For convenience in accomplishing this, virial equations of state are used in conjunction with the steady flow energy equation.

Solving the energy equation for mass flux squared at any station along the venturi axis gives (neglecting elevation changes along the axis)

$$\left(\frac{\dot{m}}{A_2}\right)^2 = \frac{2g_c\rho_2^2(h_v - h_2)}{1 - \frac{\rho_2^2 A_2^2}{\rho_v^2 A_v^2}} \qquad \text{(B-2)}$$

where subscripts v and 2 denote inlet and downstream stations, respectively, and

$\dot{m}$ = mass flow rate

A = flow area

ρ = mass density

h = enthalpy per unit mass

From measured values of inlet pressure p_v and temperature T_v, inlet values for ρ_v, h_v, and S_v (entropy) were computed using the following virial equations which are based on the equations proposed in Ref. 16 and on the Law of Corresponding States (see Ref. 17):

State equation

$$P_R = Z'\rho_R T_R \qquad \text{(B-3)}$$

Compressibility equation

$$Z' = 1 + A'_1\rho_R + A'_2\rho_R^2 + A'_4\rho_R^4 + A'_5\rho_R^5 \qquad \text{(B-4)}$$

Enthalpy equation

$$\frac{(h - h_0)}{RT} = \left[\frac{3C'_3}{T_R^3} + \frac{5C'_5}{T_R^5}\right]\left[\frac{1 - \exp(-C''_3\rho_R^2)}{C''_3}\right] + \left[B_0 + \frac{2B_1}{T_R} + \frac{4B_3}{T_R^3} + \frac{6B_5}{T_R^5}\right]\rho_R + \left[C_0 + \frac{3C_1}{2T_R} - \left(\frac{C'_3}{2T_R} + \frac{3C'_5}{2T_R^5}\right)\exp(-C''_3\rho_R^2)\right]\rho_R^2 + \left[\left(\frac{C'_3}{T_R^3} + \frac{C'_5}{T_R^5}\right)C''_3\exp(-C''_3\rho_R^2)\right]\rho_R^4 + \frac{6E_1}{5T_R}\rho_R^5 \qquad \text{(B-5)}$$

Entropy equation

$$\frac{S - S_0}{R} = \left[\frac{C'_3}{T_R^3} + \frac{2C'_5}{T_R^5}\right]\left[\frac{2}{C''_3}\right]\left[1 - \exp(-C''_3\rho_R^2)\right] - \left[B_0 - \frac{2B_3}{T_R^3} - \frac{4B_5}{T_R^5}\right]\rho_R - \left[\frac{C_0}{2} + \left(\frac{C'_3}{T_R^3} + \frac{2C'_5}{T_R^5}\right)\exp(-C''_3\rho_R^2)\right]\rho_R^2 - \ln P' \qquad \text{(B-6)}$$

where

$P_R \equiv$ reduced pressure (p/critical pressure)

$T_R \equiv$ reduced temperature (T/critical temperature)

$\rho_R \equiv$ reduced density (ρ/critical density)

$A'_1 \equiv B_0 + B_1/T_R + B_3/T_R^3 + B_5/T_R^5$

$A'_2 \equiv C_0 + C_1/T_R + C_3/T_R^3 + C_5/T_R^5$

$A'_4 \equiv (C_3 + C_5)C''_3$, $A'_5 \equiv E_1$ — for N_2 and C_2H_4

$A'_4 \equiv (C_3/T_R^3 + C_5)C''_3$, $A'_5 \equiv E_1/T_R$ — for B_2H_6

$C_3 \equiv C'_3\exp(-C''_3\rho_R^2)$

$C_5 \equiv C'_5\exp(-C''_3\rho_R^2)$

$P' \equiv$ pressure normalized by atmospheric pressure

$h_0 \equiv$ ideal gas enthalpy per unit mass

$S_0 \equiv$ ideal gas entropy per unit mass at 1 atmosphere pressure

Table B-1. Thermodynamic and virial equation constants used for N_2, C_2H_4, and B_2H_6 gases

Constant	Gas					
	N_2[a]		C_2H_4[a]		B_2H_6[b]	
Critical pressure, MN/m^2 (psia)	3.399	(492.9)	5.117	(742.15)	4.005	(580.9)
Critical temperature, K (°R)	126.26	(227.27)	283.06	(509.51)	289.83	(521.7)
B_0	0.15694		0.12107		0.032529	
B_1	−0.39800		−0.31262		−0.20765	
B_3	−0.083742		−0.15322		−0.16789	
B_5	0.0093650		0		0	
C_0	0.024350		0.040655		−0.18904	
C_1	−0.018047		−0.052715		0.32675	
C_3'	0.030135		0.053650		−0.096318	
C_3''	0.068122		0.043633		0.082774	
C_5'	0.0033110		0		0	
E_1	0.93665×10^{-4}		0.96444×10^{-4}		-4.8395×10^{-4}	

[a]Data from Ref. 17.
[b]Derived from data of Ref. 19.

and B_0, B_1, B_3, B_5, C_0, C_1, C_3', C_3'', C_5', and E_1 are constants for particular gases.

Ideal enthalpy and entropy data used for N_2, C_2H_4, and B_2H_6 were obtained from Refs. 12, 17, and 18, respectively. Values for the thermodynamic and virial equation constants and the sources for that data are listed in Table B-1.

After the gas properties were computed at the venturi entrance, Eqs. (B-2–B-6) were then utilized to compute mass flux for a range of decreasing pressures (setting $S = S_v$) so that conditions for several abitrary stations spanning the throat region were evaluated (Fig. B-2a). Thus, calculated mass flux was observed to increase to a maximum and then to decrease as the stations proceeded through the throat.[11]

One of the arbitrary stations just upstream of the approximate throat plane, as established by the maximized mass flux calculated above, was subsequently assigned as reference station x. From Fig. B-2b, it can be seen that in general

$$h_v - h_2 = (h_v - h_x) + (h_x - h_2) \qquad \text{(B-7)}$$

where h_2 represents any of the other arbitrary stations downstream of station x.

Furthermore, if $h_x - h_2$ can be expressed as a third-order polynomial function of $\rho_x^2 - \rho_2^2$ (Fig. B-2c), then

$$h_x - h_2 = K_0 + K_1(\rho_x^2 - \rho_2^2) + K_2(\rho_x^2 - \rho_2^2)^2 + K_3(\rho_x^2 - \rho_2^2)^3 \qquad \text{(B-8)}$$

and

$$\frac{dh_2}{d\rho_2^2} = K_1 + 2K_2(\rho_x^2 - \rho_2^2) + 3K_3(\rho_x^2 - \rho_2^2)^2 \qquad \text{(B-9)}$$

The coefficients $K_{0\text{-}3}$ in Eq. (B-8) were satisfactorily evaluated by standard curve-fitting methods,[12] using data for station x and three of the other stations spanning the throat; i.e., a curve was fitted to three data points.

The differential $dh_2/d\rho_2^2$ can also be obtained from Eq. (B-2) by differentiating $(m/A_2)^2$ with respect to ρ_2^2 (entropy constant) and setting the result equal to zero, representing the sonic throat condition. Thus,

$$\frac{d(\dot{m}/A_2)^2}{d\rho_2^2} = \frac{2g_c(h_v - h_2)}{\left(1 - \frac{\rho_2^2 A_2^2}{\rho_v^2 A_v^2}\right)^2} - \frac{2g_c\rho_2^2 \frac{dh_2}{d\rho_2^2}}{1 - \frac{\rho_2^2 A_2^2}{\rho_v^2 A_v^2}} = 0$$

therefore

$$\frac{dh_2}{d\rho_2^2} = \frac{h_v - h_2}{\rho_2^2\left(1 - \frac{\rho_2^2 A_2^2}{\rho_v^2 A_v^2}\right)}$$

[11]For this series of calculations, the term containing the variable $(A_2/A_v)^2$ in the denominator of Eq. (B-2) was assumed to give negligible variations in the region of the throat and was therefore assigned the constant value of $(A^*/A_v)^2$.

[12]It was also determined that an equally good fit could be obtained with the function $h_x - h_2 = B(\rho_x^2 - \rho_2^2)^k$.

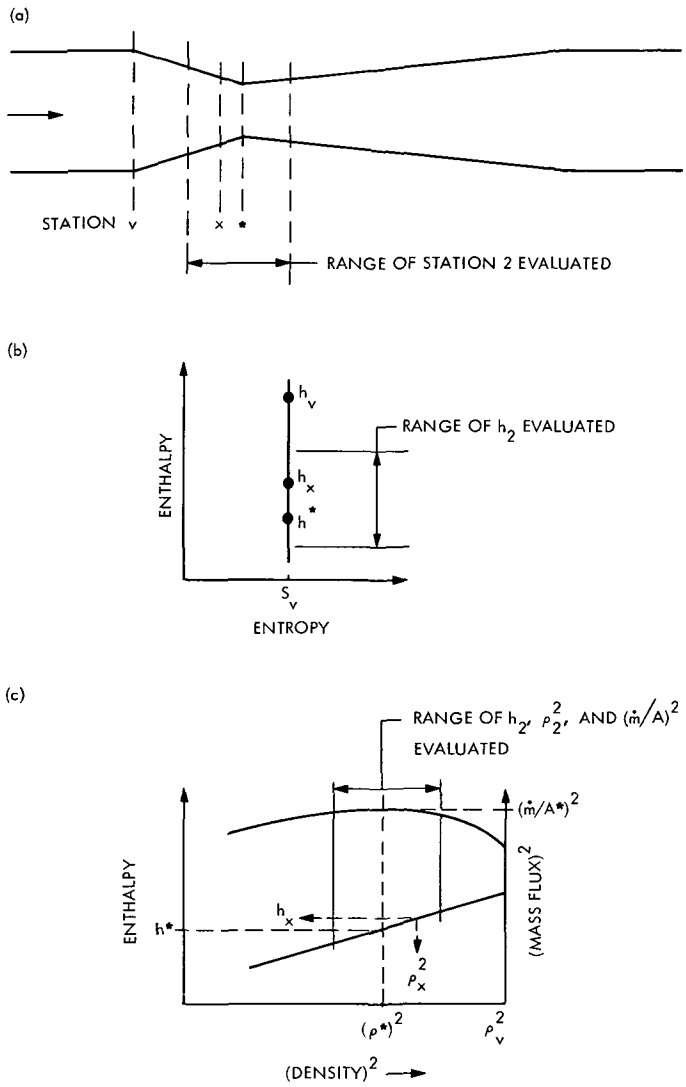

Fig. B-2. Schematic representation of expansion through sonic venturi

or, from Eq. (B-7),

$$\frac{dh_2}{d\rho_2^2} = \frac{(h_v - h_x) + (h_x - h_2)}{\rho_2^2\left(1 - \dfrac{\rho_2^2 A_2^2}{\rho_v^2 A_v^2}\right)} \tag{B-10}$$

Equating Eqs. (B-9) and (B-10) and substituting the sonic condition designation * for station 2 gives

$$K_1 + 2K_2(\rho_x^2 - \rho^{*2}) + 3K_3(\rho_x^2 - \rho^{*2})^2 = \frac{h_v - h_x + [K_0 + K_1(\rho_x^2 - \rho^{*2}) + K_2(\rho_x^2 - \rho^{*2})^2 + K_3(\rho_x^2 - \rho^{*2})^3]}{\rho^{*2}\left(1 - \dfrac{\rho^{*2}A^{*2}}{\rho_v^2 A_v^2}\right)} \tag{B-11}$$

Equation (B-11) was solved for ρ^* using standard iteration techniques. Setting $\rho_2 = \rho^*$ and $h_2 = h^*$, h^* was computed from Eq. (B-8). Finally, $\dot{m}$ was computed from

$$\dot{m} = C_d A^* \rho^* \left[\frac{2g_c(h_v - h^*)}{1 - \dfrac{\rho^{*2}A^{*2}}{\rho_v^2 A_v^2}}\right]^{1/2} \tag{B-12}$$

In practice, fuel flow calculations were performed using the standard venturi equation (Eq. B-1) for all digitally recorded time slices (~50 samples per second), as was done for oxidizer flows and other reduced data. However, fuel flows were subsequently recalculated by the more correct method outlined above for selected times, generally for the midportion and near the end of each firing. Computerized methods were used for all calculations.

IV. Combustor Operational Parameters

A. Mixture Ratio O/F

The mixture ratio was computed as follows:

$$O/F = \frac{\dot{m}_{ox}}{\dot{m}_f + \dot{m}_b} \tag{B-13}$$

where subscripts ox, f, and b refer to total oxidizer, core fuel, and barrier fuel flows, respectively.

B. Barrier Mass Fraction Z_t

The barrier mass fraction was computed as follows:

$$Z_t = \frac{\dot{m}_b}{\dot{m}_{ox} + \dot{m}_f + \dot{m}_b} = \frac{\dot{m}_b}{\dot{m}_t} \tag{B-14}$$

C. Chamber Pressure, p_{ce}

The chamber pressure was computed as follows:

$$(p_{ce})_{I,N} = \frac{(p_c)_{I,N}}{(K)_{I,N}} \tag{B-15}$$

where subscripts I and N refer to values for the injector and nozzle entrance stations of the combustion chamber, respectively, and

p_{ce} = isentropic nozzle throat stagnation pressure

p_c = measured average absolute static chamber pressure

$K_{I,N}$ = conversion factor based on one-dimensional isentropic flow:

$$K_I = (1 + \gamma M^2)\left[\frac{1}{1 + \left(\frac{\gamma - 1}{2}\right) M^2}\right]^{\gamma/(\gamma-1)}$$

$$K_N = \left[\frac{1}{1 + \left(\frac{\gamma - 1}{2}\right) M^2}\right]^{\gamma/(\gamma-1)}$$

where

γ = specific heat ratio of combustion gases

M = chamber flow Mach number

Typical values for K_I and K_N were determined to be 1.013 and 0.986, respectively, and were assumed to be constant throughout these experiments.

D. Combustion Roughness, p_c rms

This parameter was used as a measure of the fluctuating component of chamber pressure to denote combustion noise during stable firings. Its value was generated electronically from the output signal of one of the Kistler transducers, where the signal components between 10 Hz and 8 kHz were converted to a single combined rms level averaged for a 100-ms time constant throughout the firing. The averaged rms fluctuations were expressed in pressure units based on transducer calibration data.

V. Performance Parameters

A. Characteristic Velocity c*

Characteristic velocity was computed using the standard relationship

$$(c^*)_{I,N} = \frac{g_c (p_{ce})_{I,N} A_{thr}}{\dot{m}_t} \qquad \text{(B-16)}$$

where

A_{thr} = geometric nozzle throat area

B. c* Efficiency η_{c*}

This parameter was computed as

$$(\eta_{c*})_{I,N} = \frac{(c^*)_{I,N}}{[c^*_{th}]_{O/F}} \qquad \text{(B-17)}$$

where $[c^*_{th}]_{O/F}$ = theoretical c^* for measured O/F, based on one-dimensional equilibrium considerations. Theoretical values for O_2/C_2H_4 were computed using the NASA Lewis Research Center ODE computer program described in Ref. 20 with a heat of formation for C_2H_4 of 52.26 kJ (12.49 kcal/mole). Theoretical values for FLOX/B_2H_6 were taken from Ref. 1.

VI. Helium-Bleed Kistler

All high-response chamber pressure measurements were made using the so-called helium-bleed tap technique. This

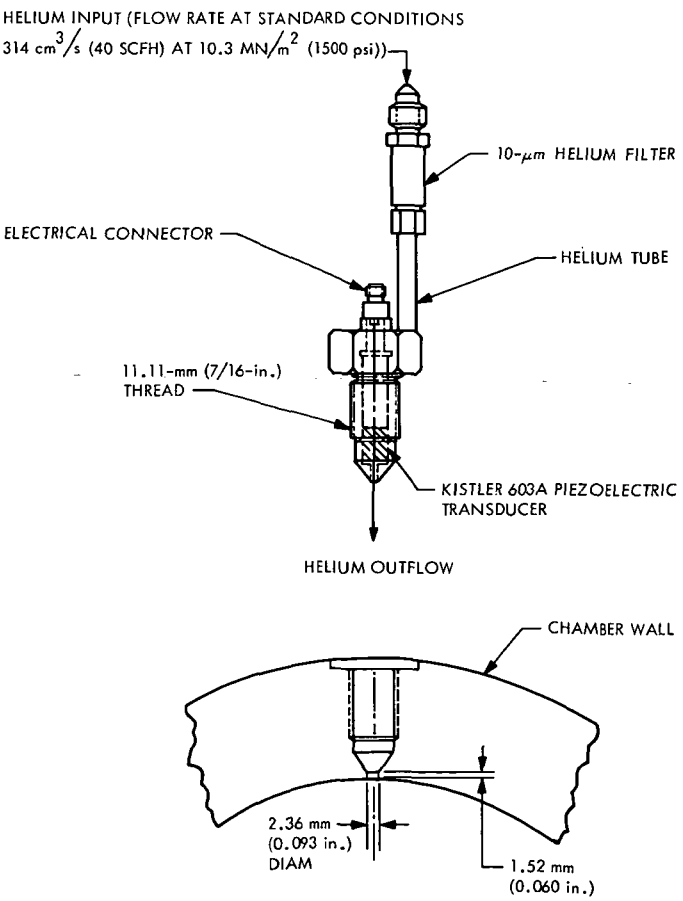

Fig. B-3. High-response helium-bleed Kistler tap configuration

technique affords thermal protection to a recessed transducer while retaining a reasonably high tap-cavity resonant frequency by virtue of the high sonic velocity for helium that flows through the cavity. Shock tube tests (see Ref. 5) of the configuration used in these experiments (Fig. B-3) indicate a rise time capability of about 20 μs with a resonant frequency of about 50 kHz. Thus a nearly flat dynamic response out to 10–15 kHz is estimated for the experimental high response measurements.

The Kistler transducer and helium-bleed adapter, as used in these experiments, were manufactured by Kistler Instrument Corp., Seattle, Wash., and PCB Piezotronics, Inc., Buffalo, N.Y., respectively.

Appendix C

Test Facilities

The O_2/C_2H_4 and FLOX/B_2H_6 firings were conducted at the JPL Edwards Test Station, Edwards Air Force Base, California, utilizing test stands B and C, respectively. Both facilities are located approximately 200 m (~600 ft) from a common control and recording center from which all firings were remotely controlled and monitored, and at which all data were recorded.

General views of the feed system for the O_2/C_2H_4 experiments are shown in Fig. C-1 (including a local control panel used during stand preparation and checkout, and the local stand shop). The foreground of Fig. C-1b shows the C_2H_4 bottle bank enclosed so that the gas supply could be warmed and maintained above its saturated vapor temperature. Figure C-2 shows the heavyweight combustor mounted and being prepared for a firing test. The massiveness of the thrust mount reflects its nominal 2 MN (~50,000 lbf) thrust capacity and not that required for this combustor.

The FLOX/B_2H_6 feed system is shown in Fig. C-3, which also includes a view of portions of the exhaust gas scrubber assembly. Major components of the fuel vaporization and heating system are visible in Fig. C-3a. Figure C-3b shows the liquid FLOX supply tank, but the vapor tank is hidden from view. A view of the combustor installation is shown in Fig. C-4.

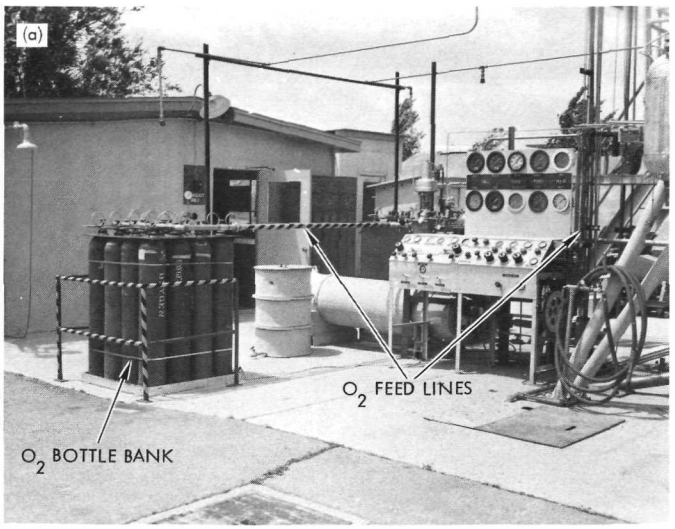

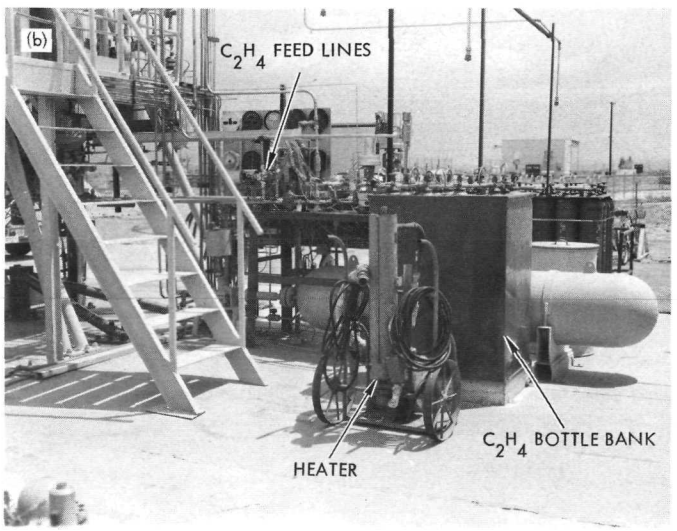

Fig. C-1. General views of O_2/C_2H_4 feed system: (a) O_2 bottle bank and feed lines and (b) C_2H_4 bottle bank (enclosed), feed lines, and heater

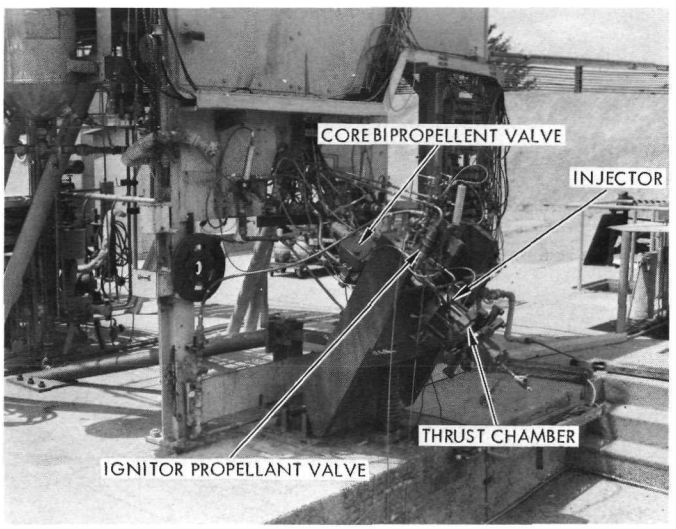

Fig. C-2. Heavyweight combustor installed in preparation for O_2/C_2H_4 firings

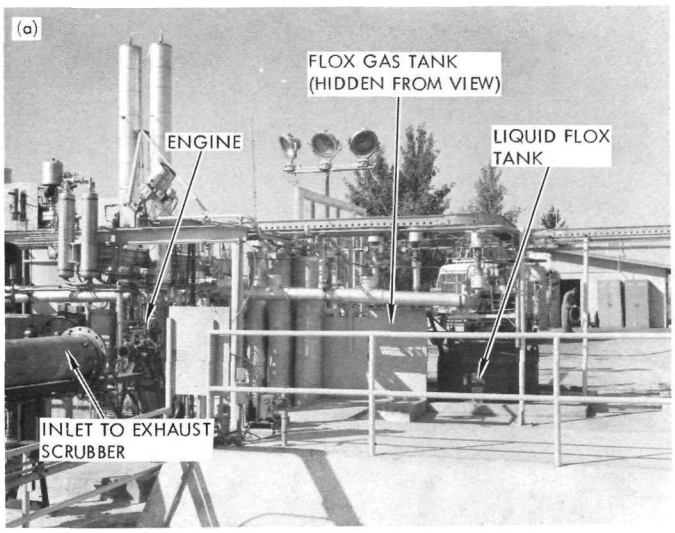

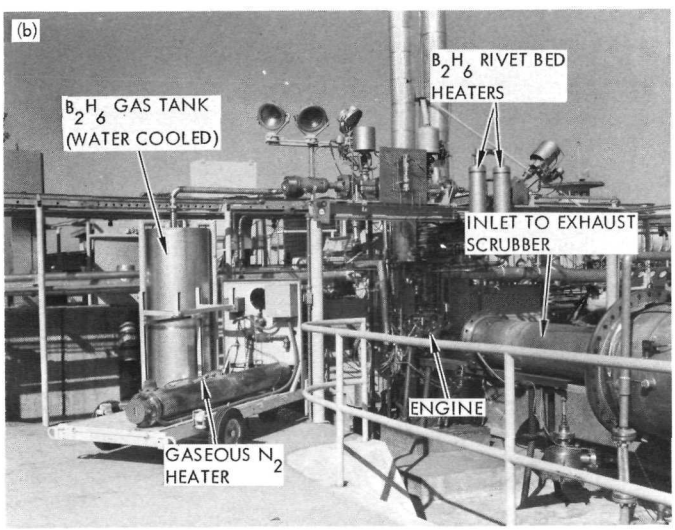

Fig. C-3. General views of FLOX/B_2H_6 feed system: (a) B_2H_6 system and (b) FLOX system

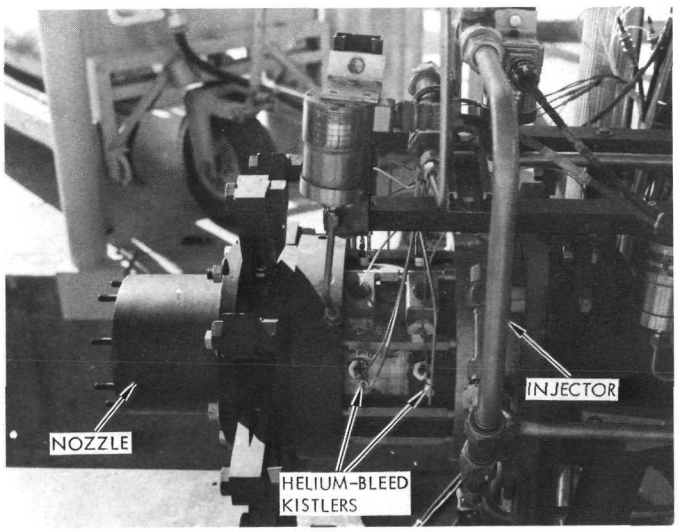

Fig. C-4. Heavyweight combustor installed in preparation for FLOX/B_2H_6 firings

References

1. Wagner, W. R., *Regeneratively Cooled Rocket Engine for Space Storable Propellants*, R-8866 (Interim Final Report, Contract NAS7-765). Rocketdyne Division, North American Rockwell Corporation, Canoga Park, Calif. (In preparation).

2. Burstein, S. Z., and Schechter, H. S., *A Study of High Frequency Nonlinear Combustion Instability in Baffled Annular Liquid Propellant Rocket Motors*, MR-7009 and 7008 (Volumes I and II of Final Report, Contract NAS7-752). Mathematical Applications Group Inc., White Plains, N. Y., Aug. 31, 1970.

3. *Combustion Stability Specifications and Verification Procedures*, prepared by the Committee on Combustion Stability Requirements and Demonstration Procedures of the JANNAF Working Group on Liquid Propellant Combustion Instability. Publication 218, Chemical Propulsion Information Agency, Silver Spring, Md., Sept. 1971.

4. Clayton, R. M., and Rogero, R. S., *Experimental Measurements on a Rotating Detonation-Like Wave Observed During Liquid Rocket Resonant Combustion*, Technical Report 32-788. Jet Propulsion Laboratory, Pasadena, Calif., Aug. 15, 1965.

5. Rogero, R. S., "Miniaturized Piezoelectric Transducer Electronics Versus Charge Amplifiers—A Comparison of the Two Systems in Vibration and Pressure Applications," presented at the ISA Aerospace Symposium, Miami, Fla., May 15–17, 1972. Instrument Society of America, Pittsburgh, Pa.

6. Clayton, R. M., Rupe, J. H., and Gerbracht, F. G., *An Experimental Correlation of the Nonreactive Properties of Injection Schemes and Combustion Effects in a Liquid Propellant Rocket Engine: Part II. Instrumentation, Experimental Apparatus, and Experimental Techniques*, Technical Report 32-255. Jet Propulsion Laboratory, Pasadena, Calif., May 15, 1967.

7. Riebling, R. W., and Powell, W. B., "Thrust-Chamber Technology for Oxygen Difluoride/Diborane Propellants," *J. Spacecraft Rockets*, Vol. 8, No. 1, pp. 4–14, Jan. 1971.

8. Tonon, T. S., Sirignano, W. A., and Harrje, D. T., *Fluid Mechanics Approach to Acoustic Liner Design*, AMS 963 (NASA CR-72807). Princeton University, Princeton, N. J., Dec. 1970.

9. Oberg, C. L., "Combustion Stabilization with Acoustic Cavities," *J. Spacecraft Rockets*, Vol. 8, No. 12, pp. 1220–1225, Dec. 1971.

10. Tang, P. K., and Sirignano, W. A., "Theoretical Studies of a Quarter-Wave Tube," AIAA paper 71-87, presented at the AIAA Ninth Aerospace Sciences Meeting, New York, N. Y., Jan. 25–27, 1971, sponsored by the American Institute of Aeronautics and Astronautics.

11. Combs, L. P., et al., *Improvement of Bombs and Pulse Guns as Combustion Stability Rating Devices*, Final Report AFRPL-TR-68-18. Rocketdyne Division, North American Rockwell Corporation, Canoga Park, Calif., Mar. 1968.

12. Hilsenrath, J., et al., *Tables of Thermal Properties of Gases*, Circular 564. U. S. National Bureau of Standards, Washington, D. C., Nov. 1, 1955.

References (contd)

13. Prydz, R., and Straty, G. C., *The Thermodynamic Properties of Compressed Gaseous and Liquid Fluorine*, Technical Note 392. U. S. National Bureau of Standards, Washington, D. C., Oct. 1970.

14. Weber, L. A., *Thermodynamic and Related Properties of Oxygen From the Triple Point to 300 K at Pressures to 330 Atmospheres*, Report 9710 A. U. S. National Bureau of Standards, Boulder, Colo., Aug. 29, 1968.

15. Waldman, B. J., *Fluorine-Hydrogen Performance Evaluation PHASE II: Space Storable Propellant Performance Demonstration*, Final Report R-6636-3 (NASA CR-72542). Rocketdyne Division, North American Rockwell Corporation, Canoga Park, Calif. Undated.

16. Benedict, M., Webb, G. B., and Rubin, L. C., "An Empirical Equation for Thermodynamic Properties of Light Hydrocarbons and Their Mixtures," *J. Chem. Phys.*, Vol. 8, pp. 334–345, Apr. 1940.

17. *Gas Engineers Handbook*, First Edition. Edited by C. George Segeler, The Industrial Press, New York, N. Y., 1966.

18. Rossini, F. D., et al., *Selected Values of Properties of Hydrocarbons*, Circular 461. U. S. National Bureau of Standards, Washington, D. C., Nov. 1947.

19. Galbraith, H. J., and Masi, J. F., *A Generalized Data Fitting Routine for the LGP-30 Computer; Application to Real Gas Properties of Diborane*, Callery Chemical Company, Callery, Pa. Undated.

20. McBride, B. J., and Gordon, S., "ICRPG One-Dimensional Equilibrium Reference Program, ODE," NASA Lewis Research Center, Cleveland, O. Undated.

NASA — JPL — Coml., L.A., Calif.

N72-30772

TECHNICAL REPORT STANDARD TITLE PAGE

1. Report No. 32-1561	2. Government Accession No.	3. Recipient's Catalog No.
4. Title and Subtitle STABILITY EVALUATION OF A ROCKET ENGINE FOR GASEOUS OXYGEN DIFLUORIDE (OF_2) AND GASEOUS DIBORANE (B_2H_6) PROPELLANTS		5. Report Date August 15, 1972 6. Performing Organization Code
7. Author(s) Richard M. Clayton		8. Performing Organization Report No.
9. Performing Organization Name and Address JET PROPULSION LABORATORY California Institute of Technology 4800 Oak Grove Drive Pasadena, California 91103		10. Work Unit No. 11. Contract or Grant No. NAS 7-100 13. Type of Report and Period Covered Technical Report
12. Sponsoring Agency Name and Address NATIONAL AERONAUTICS AND SPACE ADMINISTRATION Washington, D.C. 20546		14. Sponsoring Agency Code

15. Supplementary Notes

16. Abstract

Results of an experimental evaluation of the dynamic stability of a candidate combustor for the space storable propellants gaseous OF_2/B_2H_6 show that the combustor is unstable without supplementary damping. An analysis using a Jet Propulsion Laboratory computer program (TRDL) indicated that the uninhibited engine could be unstable. The experiments, conducted with O_2/C_2H_4 substitute propellants and with 70-30 FLOX/B_2H_6 (OF_2 simulated with FLOX), show that the uninhibited combustor has a low stability margin to starting transient perturbations, but that it is relatively insensitive to bomb disturbances. Damping cavities are shown to provide stability.

17. Key Words (Selected by Author(s))	18. Distribution Statement
Combustion Stability Propulsion, Liquid	Unclassified -- Unlimited

19. Security Classif. (of this report)	20. Security Classif. (of this page)	21. No. of Pages	22. Price
Unclassified	Unclassified	33	

38701

HOW TO FILL OUT THE TECHNICAL REPORT STANDARD TITLE PAGE

Make items 1, 4, 5, 9, 12, and 13 agree with the corresponding information on the report cover. Use all capital letters for title (item 4). Leave items 2, 6, and 14 blank. Complete the remaining items as follows:

3. Recipient's Catalog No. Reserved for use by report recipients.

7. Author(s). Include corresponding information from the report cover. In addition, list the affiliation of an author if it differs from that of the performing organization.

8. Performing Organization Report No. Insert if performing organization wishes to assign this number.

10. Work Unit No. Use the agency-wide code (for example, 923-50-10-06-72), which uniquely identifies the work unit under which the work was authorized. Non-NASA performing organizations will leave this blank.

11. Insert the number of the contract or grant under which the report was prepared.

15. Supplementary Notes. Enter information not included elsewhere but useful, such as: Prepared in cooperation with... Translation of (or by)... Presented at conference of... To be published in...

16. Abstract. Include a brief (not to exceed 200 words) factual summary of the most significant information contained in the report. If possible, the abstract of a classified report should be unclassified. If the report contains a significant bibliography or literature survey, mention it here.

17. Key Words. Insert terms or short phrases selected by the author that identify the principal subjects covered in the report, and that are sufficiently specific and precise to be used for cataloging.

18. Distribution Statement. Enter one of the authorized statements used to denote releasability to the public or a limitation on dissemination for reasons other than security of defense information. Authorized statements are "Unclassified—Unlimited," "U. S. Government and Contractors only," "U. S. Government Agencies only," and "NASA and NASA Contractors only."

19. Security Classification (of report). NOTE: Reports carrying a security classification will require additional markings giving security and downgrading information as specified by the Security Requirements Checklist and the DoD Industrial Security Manual (DoD 5220.22-M).

20. Security Classification (of this page). NOTE: Because this page may be used in preparing announcements, bibliographies, and data banks, it should be unclassified if possible. If a classification is required, indicate separately the classification of the title and the abstract by following these items with either "(U)" for unclassified, or "(C)" or "(S)" as applicable for classified items.

21. No. of Pages. Insert the number of pages.

22. Price. Insert the price set by the Clearinghouse for Federal Scientific and Technical Information or the Government Printing Office, if known.